REVIEW OF BEAM-BEAM SIMULATIONS

S. Myers

CERN, Geneva, Switzerland

1. INTRODUCTION

The interaction of particles from one beam with the electro-magnetic fields generated by the other beam (the 'beam-beam effect') has been wholly or partly responsible for the luminosity limitations observed in every electron-positron collider ever constructed. In fact an electron positron collider design which is not performance-limited by the beam-beam effect is considered to be poorly optimised.

An analytical treatment of the beam-beam effect does not yet exist; however many computer codes have been written to simulate the effect. The total computing time needed by such simulations is approximately proportional to the number of beam-beam interactions. For electron-positron storage rings it is usually sufficient to simulate for a few transverse damping times. Consequently the computing time needed to simulate smaller storage rings (where the number of beam-beam kicks per transverse damping time is high) imposes a severe limitation. For this reason, in the past, simulations tended to be oversimplified and could not therefore be expected to produce realistic results. More recently, with the advent of larger circumference storage rings and faster computers, the simulations have become more realistic and have been successful in producing results which agree with measurements.

In the following sections a review is made of the simulation techniques and simulation results. In addition a comparison is made between simulation results and experimental measurements.

1.1 The beam-beam effect

Figure 1 shows a sketch of a single particle from one beam (say electrons) under the influence of the electromagnetic fields created by the other beam (say positrons). The exact dependence of the beam-beam deflection on the displacement of the particle from the centre of charge of the bunch is indicated in Fig. 2 for the case of a LEP ribbon beam; i.e. $\sigma_x = 25\sigma_y$. Clearly the beam-beam force ($\Delta y'$) is a strongly non-linear function of the displacement; in addition y_d is compound of two constituents (ref. to Fig. 3), i.e.

$$y_d = y_{SEP} + y_A - \langle y_B \rangle \qquad (1)$$

where y_{SEP} is the separation between the reference orbits of the two beams at the collision point (This may be due to imposed separation by electro-static fields. For colliding beams $y_{SEP} = 0.$),

$\langle y_B \rangle$ is the displacement of the centre of gravity of beam B from its reference orbit,

and y_A is the displacement of a particle in beam A from its reference orbit.

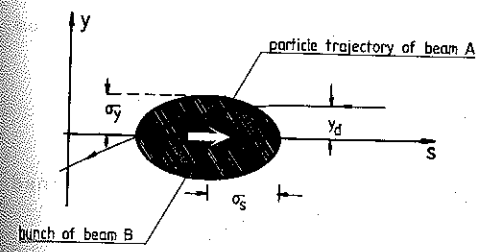

Fig 1. Particle deflection due to the beam-beam forces.

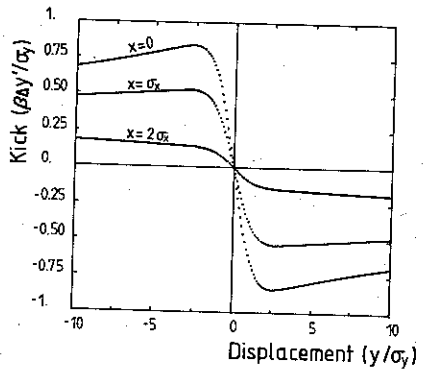

Fig. 2. Beam-beam kick as a function of displacement.

Clearly,

$$\langle y_B \rangle = y_{COB} + \langle \eta_{yB} \left(\frac{\Delta E}{E}\right)_B \rangle + \langle y_{\beta B} \rangle \qquad (2)$$

where y_{COB} is the closed orbit distortion from the reference orbit of beam B. [This may be different from that of beam A due to the Bassetti effect[1].]

$\langle \eta_{yB} \left(\frac{\Delta E}{E}\right)_B \rangle$ is the average over all particles in beam B of the product of the energy dispersion at the collision point of beam B and the energy deviation of each particle.

$\langle y_{\beta B} \rangle$ is the position of the centre of gravity of the betatron motion of beam B. This parameter must be included for simulation of the coherent beam-beam effect.

$$y_A = y_{COA} + y_{\beta A} + \eta_{yA} \left(\frac{\Delta E}{E}\right)_A . \qquad (3)$$

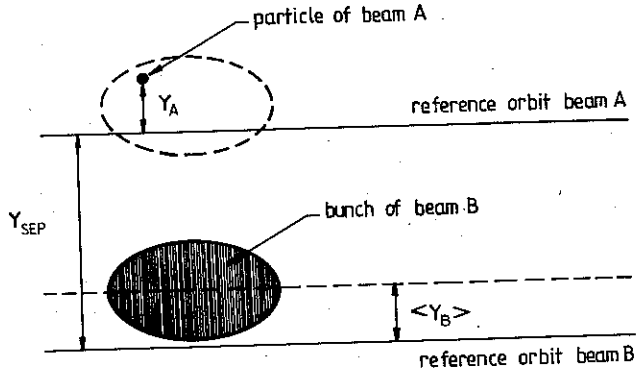

Fig. 3 Components contributing to the displacement of a particle from the centre of the 'other' bunch.

1.2 The beam-beam strength parameter (ξ)

The beam-beam strength[2] is characterized by a parameter ξ defined as

$$\xi_u \triangleq -\frac{\beta}{4\pi}\frac{\Delta u'}{u} \qquad (\text{for } u \ll \sigma_u) \qquad (4)$$

where u is either x or y

β is the betatron amplitude function at the position of the beam-beam interaction.

Hence the 'beam-beam strength parameter' (ξ) is simply proportional to the derivative of the beam-beam kick with respect to the displacement and for small displacements; in other words ξ_y is proportional to the slope of the curve in Fig. 2 at y = 0, and for x = 0.

It may seem paradoxical that the highly non-linear beam-beam effect should be characterized by this simple linear parameter. However this parameter is useful for two main reasons. Firstly it is approximately equal to the betatron tune shift (per interaction)caused by the beam-beam effect for particles with small amplitudes. This may easily be shown using the betatron rotation matrix per turn and adding a beam-beam kick given by (4), i.e.

$$\begin{pmatrix} y \\ \beta_0 y' \end{pmatrix}_{n+1} = \begin{pmatrix} \cos\mu_0 & \sin\mu_0 \\ -\sin\mu_0 & \cos\mu_0 \end{pmatrix} \begin{pmatrix} 1 & 0 \\ -4\pi\xi & 1 \end{pmatrix} \begin{pmatrix} y \\ \beta_0 y' \end{pmatrix}_n \qquad (5)$$

$$\text{therefore} \begin{pmatrix} y \\ \beta_0 y' \end{pmatrix}_{n+1} = \begin{pmatrix} \cos\mu_0 - 4\pi\xi\sin\mu_0 & \sin\mu_0 \\ -\sin\mu_0 - 4\pi\xi\cos\mu_0 & \cos\mu_0 \end{pmatrix} \begin{pmatrix} y \\ \beta_0 y' \end{pmatrix}_n$$

Here μ_0 is the unperturbed betatron phase advance between collisions. Hence the perturbed phase advance is given by

$$\frac{1}{2} \text{ (trace of perturbed matrix)} = \cos(\mu_0 + \Delta\mu_{bb})$$

i.e.
$$\cos(\mu_0 + \Delta\mu_{bb}) = \cos\mu_0 - 2\pi\xi \sin\mu_0 \qquad (6)$$

For $\Delta\mu \ll \mu_0$

$$\frac{\Delta\mu_{bb}}{2\pi} = \Delta Q_{bb} = \xi \quad . \qquad (7)$$

This relationship is only valid for tune values not too close to the integer and for small beam-beam tune shifts. The exact dependence of ΔQ_{bb} on ξ and Q_0 is shown in Fig. 4.

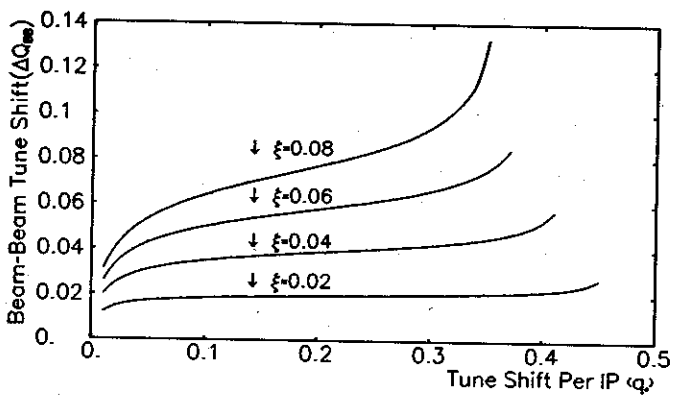

Fig. 4 Dependence of tune shift per interaction point on the tune shift between IPs for various beam-beam strength parameters (ξ).

In addition to the tune shift the β function at the interaction point is perturbed:

$$\beta \sin(\mu_0 + \Delta\mu) = \beta_0 \sin \mu_0 \ .$$

This perturbation is propagated around the ring and causes the invariation of motion to be perturbed. As a consequence the beam cross-section at the crossing point is modified.

The second reason why ξ is useful in characterising the beam-beam effect is that the higher-order non-linear terms in the expansion of the kick are proportional to the linear coefficient. (In order to illustrate this the simpler case of a round beam with a Gaussian charge distribution is treated in Appendix 1.)

For a beam with elliptical cross-section and Gaussian charge distribution the beam-beam strength parameters are

$$\xi_x = \frac{N_b r_e}{2\pi\gamma} \frac{1}{\varepsilon_x\left(1 + \frac{\sigma_y^*}{\sigma_x^*}\right)} \qquad (8)$$

$$\xi_y = \frac{N_b r_e}{2\pi\gamma} \frac{1}{\varepsilon_x\left(1 + \frac{\sigma_y^*}{\sigma_x^*}\right) k \frac{\sigma_x^*}{\sigma_y^*}} \qquad (9)$$

with

N_b	the number of particles per bunch
r_e	the classical electron radius $(e^2/4\pi\varepsilon_0 m_0 c^2)$
γ	the relativistic energy
ε_x	the horizontal beam emittance $(\frac{\sigma_x^2}{\beta})$
$\sigma_{x,y}^*$	the rms beam sizes at the collision point
k	the emittance ratio $\varepsilon_y/\varepsilon_x$.

Clearly $\xi_y = \xi_x$ when

$$k = \frac{\sigma_y^*}{\sigma_x^*} = \frac{\beta_y^*}{\beta_x^*} = \frac{\varepsilon_y}{\varepsilon_x} = k_{opt}$$

where k_{opt} is often referred to as the 'optimum coupling ratio'.

1.3 Experimental observations of the beam-beam effect

I shall only give a brief summary of the experimental observations in order to lay down a basis for comparison with the simulation results.

For beams of equal intensity and with Gaussian charge distributions colliding 'head-on' the luminosity is given by

$$\mathcal{L} = \frac{N_b^2 f_{rev} k_b}{4\pi\sigma_x^*\sigma_y^*} \qquad (11)$$

where f_{rev} is the revolution frequency,
k_b is the number of buckets.

Clearly the luminosity should increase with the square of the beam intensity. In fact this is experimentally[3] the case only for low intensities (low compared to the intensity at which the beam-beam effect is significant). At high intensity experimental evidence[3] shows that the luminosity increases only linearly (approximately) with intensity. This may only be true from (11) if the beam cross-section ($\sigma_x^*\sigma_y^*$) is also increasing linearly with intensity.

For modern electron-positron storage rings where $\sigma_x^* \gg \sigma_y^*$ ξ_y from equation (9) becomes

$$\xi_y = \frac{N_b r_e}{2\pi\gamma} \frac{\beta_y}{\sigma_x^*\sigma_y^*} \qquad (12)$$

and (11) may be rewritten

$$\mathcal{L} = \frac{N_b \gamma f_{rev} k_b \xi_y(N_b)}{2 r_e \beta_y^*} . \qquad (13)$$

From equations (12) and (13) it may be seen that at low intensities ξ_y increases linearly with current and hence the luminosity increases as the square of the current; at high currents ξ_y remains constant (or falls, due to the linear increase of $\sigma_x^*\sigma_y^*$) with current and hence luminosity increases linearly. This behaviour has been observed on nearly all electron-positron storage rings.

The beam-beam limit may therefore be interpreted as the maximum value of ξ_y which can be obtained. If this were indeed the only effect of the beam-beam then the limit imposed would be a rather soft one and dependent on the available aperture of the accelerator (The aperture should be sufficient to allow reasonable lifetimes for the perturbed beam cross-section.) Experimentally however it is usually observed that as the intensity is increased significantly beyond the point where ξ_y satu- rates, the beam lifetime suddenly becomes very low thereby imposing a limitation on the current also. This reduction in lifetime is thought to be brought about by change in the vertical distribution of the particles at large amplitudes, i.e. the 'tails' become non-Gaussian and heavily populated. This effect is the hard limit of the beam-beam effect and is difficult to study both experimentally and with simulation codes.

1.4 Importance of the beam-beam limit

Modern high-energy accelerators such as LEP tend to cost hundreds of millions of dollars to construct, commission and run. The most important performance criteria for any collider are the energy and the luminosity. It has already been stated that the maximum luminosity is dictated to a large extent by the beam-beam limit. It is therefore clear that for comparison of the performances of proposed colliding beam facilities a tool must be made available to study this effect. In addition to the luminosity limitation the beam-beam effect may have a profound influence on the background in the experimental areas and determine the way in which beams are injected into the accelerator as well as the mode of separating beams during energy ramping.

For existing colliders a proper study and understanding of the beam- beam limit will allow optimisation of the relevant machine parameters as to improve the luminosity and possibly the background rates.

1.5 Study of the beam-beam effect

There are three different techniques for studying the beam-beam effect; theoretical modelling, controlled experiments and computer simu- lation.

The progress in theoretical modelling has in the opinion of the author been rather slow due to the complexity of the problem. Most models tend to be over-simplified and it seems unlikely that such models could be used predictively in the near future. Nevertheless they may prove useful in understanding even qualitatively the parameter dependences often seen in experiments and simulation.

The use of existing accelerators to study the beam-beam effect (by means of controlled experiments) would at first sight appear to be the most realistic and straightforward approach. However difficulties arise here due to the limitation in the possible range of parameter variation and the problem of changing one parameter at a time in a complex storage ring. It should also be pointed out that configuration changes for modern accelerators can be both time-consuming and sometimes even impossible due to effects other than the beam-beam. Nevertheless existing machines can and should be used to verify the results of computer simulations in order to test the accuracy of these codes.

It is the opinion of the author that the only realistic and practical way to study the beam-beam effect (in all its detail) is by means of an exhaustive computer simulation code. Such a code should include (even in approximation) all presently known beam dynamics effects and powerful diagnostics to allow better physical understanding of the simulated results. It is the purpose of this paper to review the status of simulation of the beam-beam effect; however I do not consider it important to (and will therefore not) compare existing codes but rather state what should and can be done and what effects should be included in all codes.

2. SIMULATION TECHNIQUES (Electrons)

A beam-beam simulation 'tracks' the positions in phase space of a large number of superparticles through accelerator elements over the equivalent of many machine circumferences. In a typical simulation the elements which are 'traversed' on each turn are

(i) the accelerator lattices (between elements)
(ii) the RF stations
and (iii) the beam-beam interactions.

For electrons, where radiation damping is important, each particle is considered to lose all 'memory' of its past motion after a few transverse damping times. It is therefore sufficient to track for this limited number of turns. This is not the case for protons except at extremely high energies.

A simplified flow diagram of a typical simulation code is shown in Fig. 5. The code takes as input the machine configuration, the description of each element, various parameters related to the beam (e.g. intensity, mean values, number of bunches etc.), machine parameters (radiation integrals etc.) and the usual book-keeping parameters (required number of turns etc.).

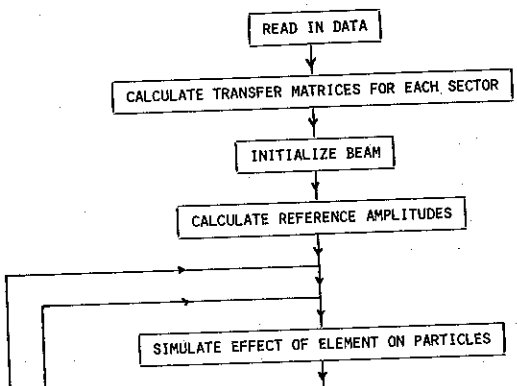

Fig. 5. Simplified flow diagram of a beam-beam simulation

Initialisation is usually performed in the following way. Given the input values of the number of superparticles, the rms beam radii and mean values in six-dimensional phase space, a Gaussian random number generator is used to set up the phase space position of each superparticle. Except in the study of injection it is usually appropriate to initialise the beams with their unperturbed dimensions (steady state equilibrum between quantum excitation and damping). These dimensions may be evaluated from the input values of the radiation integrals and the RF parameters. From a practical viewpoint this is equivalent to simulating a situation where the bunches have been circulating (but not interacting) long enough to

reach a steady state before they are instantaneously brought into collision (at the beginning of the computer run).

The machine configuration may be described as an arbitrary sequence of sectors, each sector consisting of a machine element followed by a length of lattice. The following sections describe the types of element and the transfer through a length of lattice.

2.1 Traversal of a length of machine lattice

Ideally a length of lattice would consist of a repetitive series of different types of magnet (dipoles, quadrupoles, sextupoles etc. plus the higher order pole content of each). However due to computer limitations, tracking of a large number of particles through such a structure is at present totally impractical. For this reason it is customary to use other single- (or few-) particle programs to do pre-processing of the accelerator configuration by orbit parameters (β function, phase advances etc.) as a function of azimuthal position.

In addition to the orbit parameters the synchrotron radiation due to the magnets is evaluated and output as synchrotron radiation integrals[6] which allow calculation of the equilibrium beam sizes. Hence in most beam-beam simulation codes the traversal of a length of lattice is simulated using quasi-linear betatron and synchrotron transfer matrices.

2.1.1 Betatron transfer matrix

The linear betatron transfer matrix from position 1 to position 2 for a single plane is given by

$$\begin{pmatrix} x \\ x' \end{pmatrix}_2 = \begin{pmatrix} t_{11} & t_{12} \\ t_{21} & t_{22} \end{pmatrix} \begin{pmatrix} x \\ x' \end{pmatrix}_1 \qquad (14)$$

where

$$t_{11} = \sqrt{\frac{\beta_2}{\beta_1}}\,(\cos\mu_{12} + \alpha_1 \sin\mu_{12})$$

$$t_{12} = \sqrt{\beta_1\beta_2}\,\sin\mu_{12}$$

$$t_{21} = \frac{\cos\mu_{12}[\alpha_1-\alpha_2] - \sin\mu_{12}[1+\alpha_1\alpha_2]}{\sqrt{\beta_1\beta_2}} \qquad (15)$$

$$t_{22} = \sqrt{\frac{\beta_1}{\beta_2}}\,(\cos\mu_{12} - \alpha_2 \sin\mu_{12})$$

and μ_{12} is the betatron phase advance from 1 to 2

$$\alpha = -\frac{1}{2}\frac{d\beta}{ds}\,.$$

For non-zero chromaticity

$$Q' = \Delta\mu/\left(2\pi\,\frac{\Delta E}{E}\right) \neq 0 \qquad (16)$$

the phase advance between elements is dependent on the relative energy deviation of the particle. In this case each particle, having a different $\Delta E/E$ has a different matrix. This is one form of tune modulation at harmonics of the synchrotron frequency. The other, which does not require chromaticity, is caused by the differences in path lengths (and hence betatron phase) for particles of different energy. This effect will be discussed in a later section.

The effect of tune dependence on amplitude caused by non-linearities may be approximately simulated by making the phase advance a function of the calculated betatron invariant amplitude of each particle.

It may be appreciated that any phenomena which requires that the elements of the transfer matrices be evaluated inside the number of particles loop will greatly increase the computer time. For this reason it is wise to include such phenomena as options which may be excluded at will.

2.1.2 Longitudinal motion

The longitudinal phase plane motion of particles traversing an accelerator lattice is affected by energy loss due to radiation and by a longitudinal 'drift' between particles of different energy. These effects may be approximated by

$$\Delta E_{rad} = a_0 + a_1 \Delta E \qquad (17)$$

and

$$\Delta\phi_{RF} = \frac{h\Delta\ell}{\gamma_t^2 R}\frac{\Delta E}{E} \qquad (18)$$

where a_0 is the average energy loss over the length of lattice
ΔE is the energy deviation of each superparticle
$\Delta\phi_{RF}$ is the phase slip between the particle and the RF wave (in RF radians)
h is the harmonic number of the RF
$\Delta\ell$ is the length of the lattice
γ_t is the transition energy of the accelerator
and R is the average radius (circumference/2π)

In equation (17) the coefficient a_1 is related to the normal longitudinal damping α_E by

$$a_1 = \frac{\alpha_E \Delta\ell}{\pi f_{rev} R} \qquad (19)$$

where α_E is calculated from the input values of the radiation integrals.

For the study of non-linear damping produced for example by higher-order non-linear wiggler magnets[5] equation (17) contains higher-order terms in ΔE.

2.1.3 Quantum excitation and damping

The longitudinal damping in an electron storage ring occurs in the machine lattice and may be approximately simulated by equation (17). In the transverse plane the damping is actually caused by the replacement of energy losses which occur in the lattice by an energy gain in the RF sections. Hence there are two possibilities to simulate damping. The first and simplest is to multiply the transfer matrix elements t_{ij} by a damping factor

$$\exp\left\{-\alpha_u \frac{\Delta\ell}{\beta c}\right\}$$

with α_u the damping coefficient $\left(\frac{1}{\tau_u}\right)$ evaluated from the radiation integrals
and βc the beam velocity.

The second alternative is to include the damping where it actually occurs, in the accelerating stations. This is treated in the section on RF station traversal.

In circular electron accelerators the particles emit many energy quanta per turn. The random nature of these emissions causes diffusion in all three phase planes. In the transverse phase planes the diffusion results from energy losses at positions where the energy dispersion

$$\eta_u = \frac{\Delta u}{\Delta E/E}$$

is non zero.

It can be shown[6] that the diffusion rate is given by

$$D_u \equiv \frac{d}{dt}\langle A^2 \rangle = \mathcal{N} \langle u^2 \rangle \qquad (20)$$

where A is the peak amplitude of the motion
$\mathcal{N}_u$ is the number of events like u per second
u is the magnitude of the emission.

Due to computer limitations it is usually impractical to simulate the full number ($\mathcal{N}$) of emissions per unit time; this is particularly true at high energies for electrons.

For simulation of quantum excitation with n_t quanta emitted per [illegible] the diffusion rate is maintained constant if the mean square value of the magnitude of the quanta is increased, i.e.

$$\langle u^2 \rangle_{sim} = \frac{D_u \, \Delta \ell}{\beta c \, n_t} . \qquad (21)$$

The steady state mean square beam size (σ^2_{ss}) is obtained when the diffusion and damping rates sum to zero, i.e.

$$D_u = 4\alpha_u \sigma^2_{ss}$$

where σ_{ss} may refer to x, z or ΔE.

Hence

$$\langle u^2 \rangle_{sim} = \frac{4\alpha_u \sigma_{ss}^2 \Delta\ell}{n_t \beta c} . \qquad (23)$$

Equation (23) gives the mean square magnitude of the simulated quanta which will result in the correct diffusion rate when there are n_t quanta emitted per lattice length $\Delta\ell$. In simulation codes a random number generator [variance given by (23)] is called n_t times per $\Delta\ell$ and the random value is added to the appropriate phase plane co-ordinates.

2.2 Traversal of RF accelerating cavities

The accelerating system of an electron storage ring usually consists of many multi-cell, high-Q, resonant cavity, structures which are distributed over selected regions of the machine circumference. Due to their distribution in real space they are also distributed in betatron space. The purpose of the cavities is twofold; firstly to replenish the energy lost due to synchrotron radiation and secondly to provide a longitudinal potential well (or RF bucket) which is sufficiently large to ensure a reasonable quantum lifetime in the presence of quantum excitation.

For very large storage rings (such as LEP) it is impractical to simulate the real situation of many hundreds of cells distributed over several betatron wavelengths. In simulation codes the accelerating system is usually represented by a few RF stations located at chosen positions around the accelerator circumference.

2.2.1 Longitudinal motion

Each superparticle which traverses an RF station experiences energy changes due to the externally applied fields in the cavity gaps and the summation of the longitudinal wakefields set up by all superparticles in time advance of itself.

The externally applied fields are usually given as input in the form of the required RF voltage per turn (V_{RF}) and the RF stable phase angle (ϕ_s). These parameters may also be evaluated inside the code, given the beam parameters and the required quantum lifetime, i.e. the energy change due to crossing an RF station is

$$\Delta E_{RF} = eV(\phi,\phi_s) - eV_\ell \qquad (24)$$

where $V(\phi,\phi_s)$ is the voltage at the station

ϕ is the RF phase angle of the particle

V_ℓ is the 'wake' voltage seen by the particle and is evaluated as

$$V_\ell = \frac{i_b N_{CELL}}{N_s f_{rev}} \sum_{j=1}^{N_s} W_\ell(\Delta t_j) + \frac{W_\ell(o)}{2} \qquad (25)$$

with i_b the current per bunch (A)

N_{CELL} the number of cells in the simulated RF station

N_s the number of superparticles

$W_\ell(t)$ the delta function longitudinal wakefield per cell[7]; this is usually evaluated from RF structure programs[8]

Δt_j is the time difference between each superparticle and the superparticle under scrutiny; Δt is positive for superparticles ahead of the excited particle.

For a normal RF system

$$V(\phi,\phi_s) = \hat{V} \sin(\phi + \phi_s) \qquad (26)$$

where $\hat{V}$ is the peak voltage per station.

The voltage function may also take account of higher harmonic[9] cavities etc.

2.2.2 Transverse motion

In the case where the damping is included in the machine lattice, the change in betatron motion of a particle due to traversal through an RF station is simply

$$\Delta u = - \eta_{uRF} \frac{\Delta E_{RF}}{E} \qquad (27)$$

and

$$\Delta u' = eV_t/E \qquad (28)$$

where u refers to the betatron displacement (horizontal or vertical)

η_{uRF} is the energy dispersion at the RF; this may vary from RF station to station

ΔE_{RF} is the energy gain in the station [equation (24)]

It is clear that coupling from the longitudinal to the transverse motion (synchro-betatron coupling) is brought about by the energy dispersion at the RF station.

In equation (28) V_t is the transverse voltage due to the transverse wakefield and is given by

$$V_t = \frac{i_b N_{CELL}}{N_s f_{rev}} \sum_{j=1}^{N_s} W_t(\Delta t_j) \frac{d_j}{r_{tube}} \qquad (29)$$

with $W_t(t)$ the delta function transverse wakefield evaluated[7] (using RF structure programs) at the cavity tube radius (r_{tube})

d_j is the position of the particle which induced the wakefield

It is worthwhile to point out that d_j may be the superposition of the betatron displacement (u_j), the energy motion ($\eta_{uRF} \cdot \Delta E_j/E$), and the closed orbit displacement at the cavity location. In this way synchro-betatron resonances due to dispersion at the cavities and wakefields may be simulated.

In a pure beam-beam simulation the wakefield effects may be ignored; however since it will be shown later that the beam-beam limit is dependent on many parameters it is wise to have the capability of including all known effects. Of course in a computer code the wakefield effects can be included as an option and may therefore easily be switched on and off.

For the case where the betatron damping is to occur at the RF station equation (28) becomes

$$\Delta u' = \frac{eV_t}{E} - \frac{\Delta E_{RF}}{E} u' \, . \qquad (30)$$

A simple derivation of this expression is given in Appendix 2.

4.4 Beam-beam traversal

When two bunches collide the individual particles of each bunch are influenced by the electro-magnetic forces produced by the other bunch. Transversely the particles experience deflecting fields whilst longitudinally there is an energy loss due to 'beamstrahlung'.

2.3.1 Evaluation of the beam-beam kicks

In electron storage rings the unperturbed charge distribution is Gaussian in all six dimensions, i.e. the volume charge distribution is

$$\rho_v(x,y,s) = \frac{N_b e}{(2\pi)^{\frac{3}{2}} abc} \exp\left\{-\frac{x^2}{2a^2} - \frac{y^2}{2b^2} - \frac{s^2}{2c^2}\right\} \qquad (31)$$

where a, b, c are the standard deviations in x, y and s.

It has been shown[10] that the electric potential produced by this distribution is

$$\phi(x,y,s) = \frac{N_b e}{4\pi^{\frac{3}{2}} \varepsilon_0} \int_0^\infty \frac{\exp\left\{-\frac{x^2}{2a^2+q} - \frac{y^2}{2b^2+q} - \frac{s^2}{2c^2+q}\right\} dq}{[(2a^2+q)(2b^2+q)(2c^2+q)]^{\frac{1}{2}}} \qquad (32)$$

The integrated transverse angular deflection received by a particle crossing a charged beam is given by

$$\Delta\left(\frac{du}{ds}\right) = \frac{e}{\gamma m_0 c^2} \int_{-\infty}^{\infty} E_u ds = -\frac{e}{\gamma m_0 c^2} \int_{-\infty}^{\infty} \frac{\delta\phi}{\delta u} \cdot ds \qquad (33)$$

where E_u is the transverse electric field generated by the beam.

Differentiating (32) gives the beam-beam kick. For example in the vertical plane for particles of opposite charge

$$\Delta y' = -\frac{2Nr_e y}{\gamma\sqrt{\pi}} \int_{-\infty}^{\infty} \int_0^\infty \frac{\exp\left\{-\frac{x^2}{(2a^2+q)} - \frac{y^2}{(2b^2+q)} - \frac{s^2}{(2c^2+q)}\right\} dq \cdot ds}{(2a^2+q)^{\frac{1}{2}}(2b^2+q)^{\frac{3}{2}}(2c^2+q)^{\frac{1}{2}}} \qquad (34)$$

where r_e is the classical electron radius $(e^2/4\pi\varepsilon_0 m_0 c^2)$.

Equation (34) and its counterpart for the x direction are the beam-beam kick equations in their full three-dimensional form. To use these equations in a beam-beam simulation requires numerical evaluation of the

double integral in equation (34) once per plane for each beam-beam crossing. This has in fact been done in some simulation codes but is extremely computer-time-consuming. One possible way to speed this up is to tabulate values of $\Delta x'$ and $\Delta y'$ as a function x, y, a, b, c and use interpolation to evaluate the kicks on each passage. This considerably speeds up the calculation but becomes slow again once one attempts to do 'strong-strong' simulations where the a and b change during the course of the simulation. In this case new tables have to be evaluated each time a significant change in a or b is observed.

The dependence on the longitudinal co-ordinate (s) may be eliminated by integrating equation (31) over all s, i.e.

$$\rho_s(x,y) = \frac{N_b e}{2\pi ab} \exp\left\{ -\frac{x^2}{2a^2} - \frac{y^2}{2b^2} \right\} . \qquad (35)$$

In this case the potential is

$$\phi(x,y) = -\frac{N_b e}{4\pi\,\varepsilon_0} \int_0^\infty \frac{1 - \exp\left\{ -\frac{x^2}{(2a^2+q)} - \frac{y^2}{(2b^2+q)} \right\}}{(2a^2+q)^{\frac{1}{2}}(2b^2+q)^{\frac{1}{2}}}\, dq \qquad (36)$$

and the vertical kick is

$$\Delta y' = -\frac{2N_b r_e y}{\gamma} \int_0^\infty \frac{\exp\left\{ -\frac{x^2}{(2a^2+q)} - \frac{y^2}{(2b^2+q)} \right\}}{(2a^2+q)^{\frac{1}{2}}(2b^2+q)^{\frac{3}{2}}}\, dq . \qquad (37)$$

Numerical evaluation of equations (34) and (37) (for both planes) showed that for typical electron storage ring parameters where $\sigma_s \gg \sigma_u$ the simpler two-dimensional kick of equation (37) is an extremely good approximation; the largest error over a wide range in x, y, σ_x, σ_y was 0.2%. It was therefore concluded that the two-dimensional form was perfectly acceptable for simulation of the beam-beam interaction. Equation (37) can also be written[11] as (for a > b)

$$\Delta y' = -\frac{N_b r_e}{\gamma}\sqrt{\frac{2\pi}{a^2-b^2}}\,\mathcal{R}\left[w\left(\frac{x+iy}{\sqrt{2(a^2-b^2)}}\right) - \exp\left\{-\frac{x^2}{2a^2}-\frac{y^2}{2b^2}\right\}\cdot w\left(\frac{x\frac{b}{a}+iy\frac{a}{b}}{\sqrt{2(a^2-b^2)}}\right)\right] \qquad (38)$$

with the x kick given by the imaginary part of the square brackets and where w(A+iB) is the complex error function.

Although equation (38) appears more cumbersome than (37) it is nevertheless much faster to compute. In addition, and even more important, the variables of the complex error function (A and B) can be written as functions of x, a and b and y, a and b respectively. This gives the possibility of evaluating the beam-beam kicks using interpolation of one set of tables of the complex error function independent of the changing values of a and b, i.e. strong-strong simulation needs the same computing time as strong-weak. For simulation codes this is a very important property of the complex error function form of the beam-beam kick.

2.3.2 Energy loss due to beam-beam interaction

The rate of loss of energy by radiation is given by the classical equation (for the vertical plane say)

$$\frac{dU_y}{dt} = \frac{2}{3}\frac{r_e c\,\gamma^2 F_y^2}{(m_0c^2)}$$

where F_y is the vertical deflecting force = $2eE_y$.

Thus the energy loss per beam-beam collision due to the vertical beam-beam kick is

$$U_{ybb} = \frac{4}{3}\frac{e^2 r_e \gamma^2}{(m_0c^2)}\int_{-\infty}^{\infty} F_y^2 ds = \frac{2e^2 r_e \gamma^2}{3\sqrt{\pi}\,\sigma_s (m_0c^2)}\left[\int_{-\infty}^{\infty} E_y de\right]^2$$

for a Gaussian distribution, and from (33)

$$\Delta y' = \frac{e}{\gamma m_0 c^2} \int_{-\infty}^{\infty} E_y \, ds \quad .$$

Hence

$$U_{ybb} = \frac{2r_e(m_0c^2)\gamma^4 \, \Delta y'^2}{3\sqrt{\pi}\,\sigma_s} \quad . \tag{41}$$

The total energy loss due to a beam-beam crossing is

$$U_{bb} = \frac{2r_e(m_0c^2)\gamma^4}{3\sqrt{\pi}\,\sigma_s} \{\Delta x'^2 + \Delta y'^2\} \tag{42}$$

where $\Delta x'$ and $\Delta y'$ are evaluated from (38).

2.3.3 Transverse motion

In equation (38) the beam-beam kick is given as a function of the total displacements (x and y) and the total beam sizes (a and b). As previously stated the total vertical displacement between the excited particle and the centre of the perturbing bunch is given by equations (1), (2) and (3) (section 1.1).

$$y_d = y_{SEP} + y_{COA} + y_{\beta A} + \eta_{yA} \left(\frac{\Delta E}{E}\right)_A - y_{COB} - \langle \eta_{yB} \left(\frac{\Delta E}{E}\right)_B \rangle - \langle y_{\beta B} \rangle \tag{43}$$

and a similar equation for x_d.

The total beam sizes a and b are simply the quadratic addition of the beam sizes due to synchrotron and betatron motion, e.g.

$$b^2 = \sigma_y^2 + \langle \left(\eta_{yI} \frac{\sigma_E}{E}\right)^2 \rangle \tag{44}$$

where η_{yI} is the vertical dispersion at the interaction point. For most storage rings (where $\beta_y \gg \sigma_s$) the betatron rms radii may be assumed to good approximation to remain constant over the interaction length of the bunches. In fact in equation (38) this has already been assumed. However in general

$$\beta(s) = \beta^* \left(1 - \frac{\Delta s^2}{\beta^{*2}}\right) \qquad (45)$$

where β^* is the betatron amplitude at the nominal interaction point

Δs is the distance from the nominal interaction point.

and $\sigma_y(s) = \sqrt{\varepsilon_y \beta_y(s)}$ therefore varies across the I.P. To properly simulate this effect requires the use of the equation (34), evaluated numerically with the correct variation of a and b with s. As previously stated however for most storage rings this effect is small.

The changes in betatron co-ordinates are therefore simulated by (vertically again)

$$\Delta y = - \eta_{yI} \left(\frac{U_{bb}}{E} + \frac{\Delta E}{E}\right) \qquad (46)$$

and $\Delta y'$ given by equation (38).

2.3.4 Longitudinal motion

The changes in longitudinal phase plane co-ordinates are trivial:

$$\Delta E_{bb} = U_{bb} \qquad (47)$$

and

$$\Delta \phi_{RF} = 0 .$$

3. SIMULATING INSTRUMENTATION AND DIAGNOSTICS

The use of computer simulation is usually only resorted to when there is no analytical solution possible. It is therefore difficult to know what type of behaviour to expect and to understand the physics behind such behaviour. As a simple example of this, it is clear that in a strong strong simulation the real 'blow-up rate' ($d\sigma/dt$) should not be damped by averaging the beam size over a period of time much longer than the growth rate. On the other hand updating the beam size (and the beam-beam forces) too often may produce effects due to statistical fluctuations which may result from the reduced number of particles. There is no real solution (known to the author) to this dilemma other than trial and error.

However, considerable insight and understanding of the beam behaviour may result if sufficient diagnostics are built into the computer code. To write a simulation code without sufficient built-in self-analysis would be as shortsighted as to build an accelerator without instrumentation or diagnostics. This 'simulated diagnostics and instrumentation' involves evaluating as a function of time all relevant beam parameters; the σ's and mean values in all dimensions, the luminosity, the invariants of motion etc. In addition to this one also needs spectral analysis of the coherent motion, histograms of distribution in tune, amplitude etc.

In the following sections it may be appreciated that such simulated instrumentation is invaluable for understanding and giving insight to the simulated behaviour of the beams.

4. REVIEW OF SIMULATION RESULTS

Clearly, all the effects described in section 2 can be included in any simulation code. However because of computer limitations many codes have been written which approximate or even ignore many of these phenomena in the belief that they are unimportant for the beam-beam effect. The number and type of effects which have been approximated or eliminated can have a profound effect on the simulation results. It is therefore of the utmost importance that the 'contents' of the simulation code be fully understood before too much importance is attached to the results. For example it is unrealistic to expect a 'weak-strong' simulation to predict the luminosity and even more unrealistic to expect it to be able to see the 'flip-flop effect'. Likewise any simulation which ignores or approximates the longitudinal motion is blind to the synchro-betatron effects.

In Appendix 3 a brief resumé of the published contents of the most recent simulation codes[12,13,14,15] is given. It is not unlikely however that some additional effects have in the meantime been added to these codes and have not yet been published. I make my excuses now for any misinterpretation of the published descriptions of these codes.

The beam-beam effect is influenced by many machine parameters and by the inter-relation between these parameters. In the following subsections are given the published dependence on the beam intensity, the machine tune, the number of bunches, the beam energy, the bunch length, β^*, the residual chromaticity and the machine errors. In addition to

the normal case of initially equal colliding beams, the effect of colliding unequal beams and the effects of injection, accumulation, energy ramping and bringing the beams into collision are presented.

4.1 Varying the machine tune

For existing accelerators the machine tune can usually be readily varied over a reasonable range in the non-integer part. For this reason much effort has gone into attempts to minimise the beam-beam effect (i.e. maximise the luminosity) by varying the horizontal and vertical machine tunes. However one should be aware when looking at results of tune variation that the integer tune can also influence the beam-beam effect for two main reasons. Firstly the tune shift per collision point is influenced both by the number of collision points and the integer tune. Secondly beam-beam coupling resonances require that the integer tunes, non-integer tunes and the number of bunches are related.

Examples of the simulated vertical beam sizes (normalised) as a function of tune [taken from ref. 12)] for typical PETRA parameters is shown in Fig. 6 and Fig. 7 for different integer tunes.

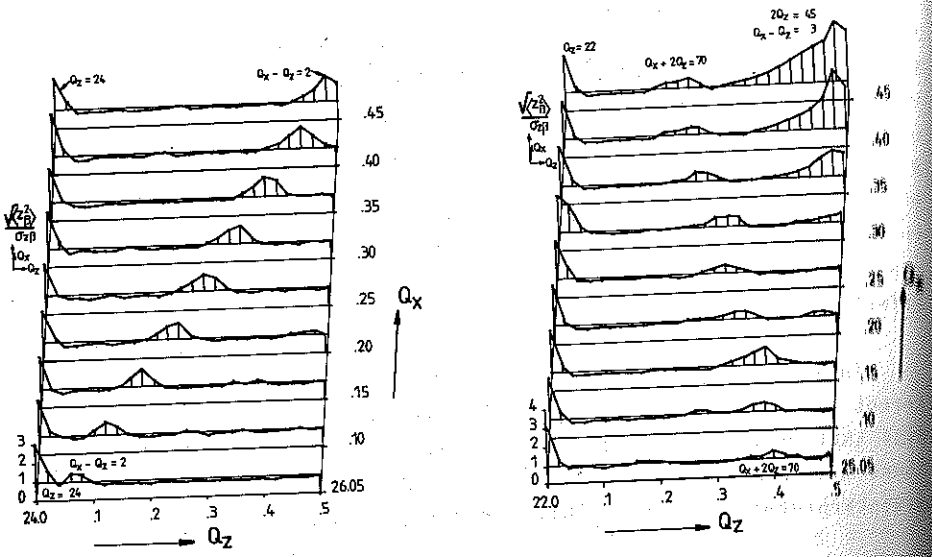

Figs. 6 and 7. Simulated beam sizes as function of betatron tunes (PETRA)

These plots are without 'machine errors' and show that, although the blow-up factor is small, the dependence of vertical beam size on vertical tune is influenced by the integer value of the vertical tune and the integer and non-integer value of the horizontal tune.

Figure 8 [taken from ref. 13)] shows the 'swamp diagram' where darker areas represent higher luminosity. This plot is done for typical CESR parameters and indicates that there are few regions of excellent luminosity in the two-dimensional tune diagram. There is no evident symmetry in this plot suggesting perhaps that a wider range in tunes would have been instructive. It should be pointed out that this swamp diagram was done for the following conditions.

$$\xi_{vo} = 0.08, \quad \xi_{ho} = 0, \quad \eta_x = 0, \quad \eta_y^* = 0$$

and as previously stated this simulation did not include 'errors'.

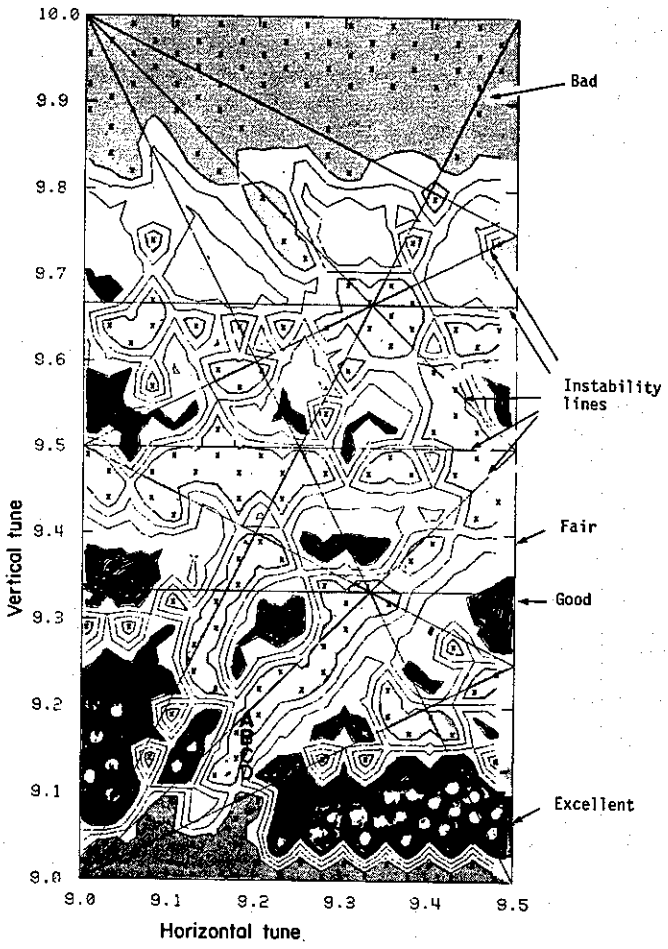

Fig. 8. Luminosity as function of betatron tunes (CESR).

The luminosity dependence on vertical tune [taken from ref. 14)] over a range of eight integers (i.e. a range of a full integer tune advance between IP's) is shown in Fig. 9. Many of the dips in luminosity can be

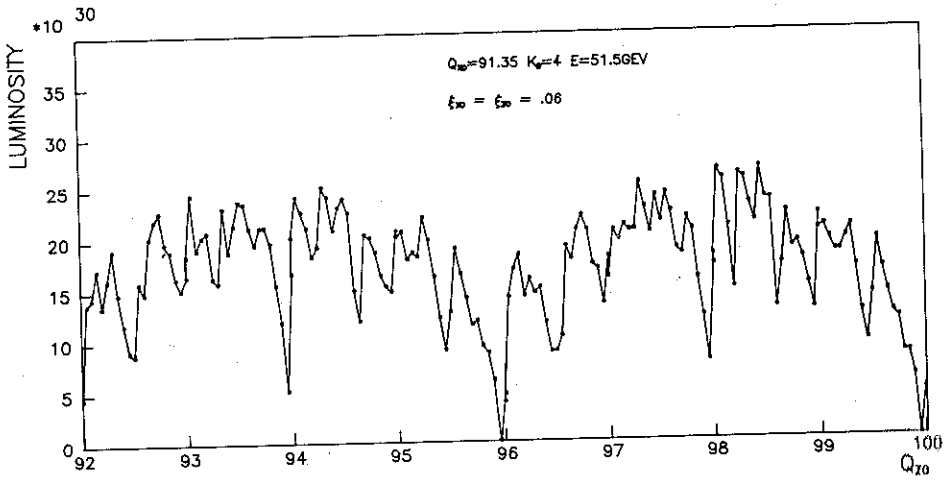

Fig. 9. Luminosity as a function of tune (LEP).

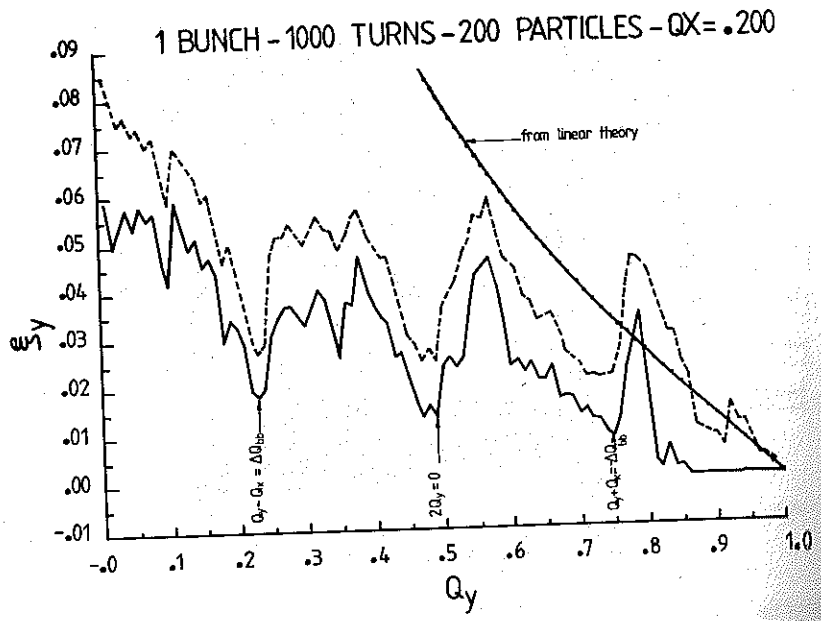

Fig. 10. Luminosity as a function of tune (LEP).

at least approximate
can be seen from th
four integers in tu
could be blind to a
ned. Similar plot
though not exhaustiv
due to the differenc
tical provided the
differences in integ

Figure 10 (ta
limit ξ_y as a funct
bunch per beam.
nances.

Figure 11 [ref.
over the optimum in
two plots each one
electrons or positro

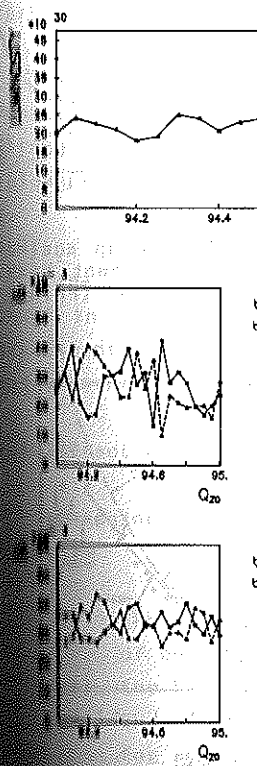

Fig. 11. Beam para
function
tune.

at least approximately accredited to beam-beam systematic resonances. It can be seen from this plot that there is an approximate periodicity over four integers in tune. However it is not a perfect periodicity and one could be blind to a good integer tune range if the full range is not scanned. Similar plots were obtained for the horizontal tune variation (although not exhaustively) and it was found that the predominant effect was due to the difference in the non-integer tunes between horizontal and vertical provided the beam-beam coupling resonances were avoided by avoiding differences in integer tune of modulo the number of bunches.

Figure 10 (taken from ref. 15) shows the variation of the beam-beam limit ξ_y as a function of machine tune over an integer range and for one bunch per beam. This plot clearly shows the beam-beam coupling resonances.

Figure 11 [ref. 14)] shows how the relevant parameters vary with tune over the optimum integer tune range found from Fig. 9. Where there are two plots each one represents the behaviour of one of the beams (either electrons or positrons).

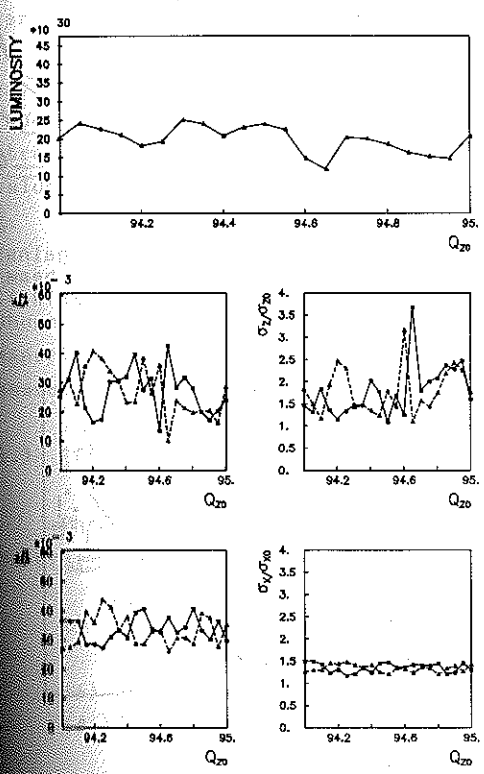

Fig. 11. Beam parameters as a function of vertical tune.

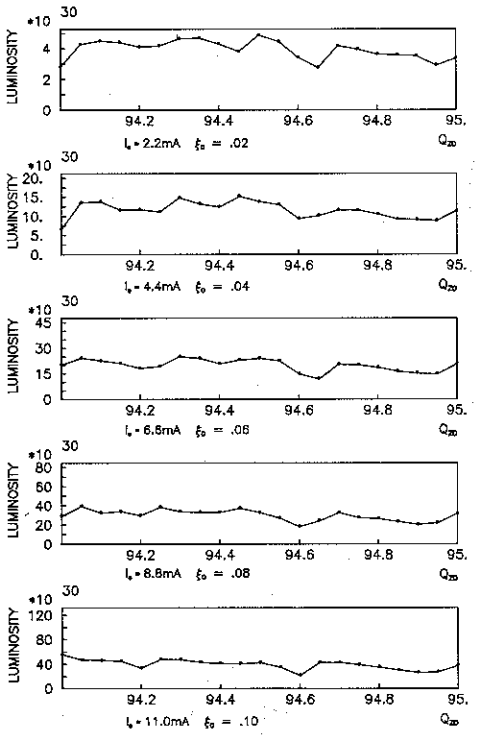

Fig. 12. Luminosity as a function of vertical tune for different intensities (LEP).

It can be seen from this that the horizontal blow-up factor is small and independent of the vertical tune. This clearly indicates that the luminosity dips are caused by vertical beam blow-up. Another interesting feature of this graph is that when one beam becomes badly blown up the other beam suffers no blow-up whatever. This is the first indication of the flip-flop to be discussed later.

4.2 Varying the beam intensity

It has been observed in nearly all electron-positron storage rings that the luminosity increases quadratically with beam current up to a certain intensity level. Beyond this intensity the luminosity increases less rapidly and finally at higher intensities the luminosity increase becomes linear.

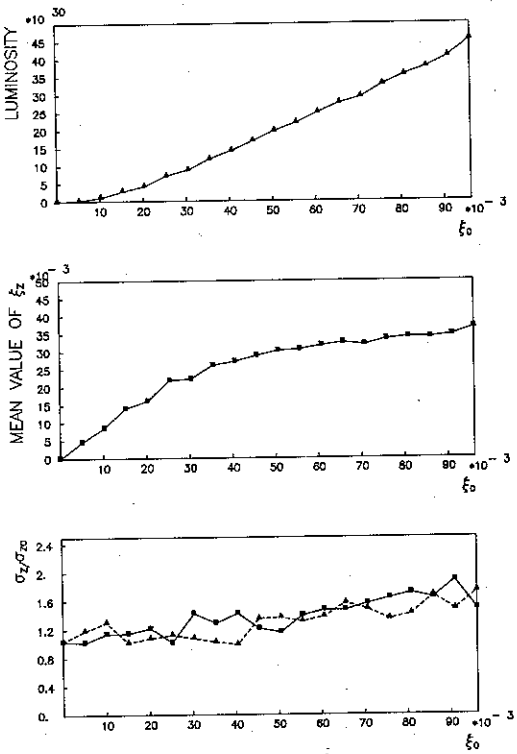

Fig. 13. Beam parameters as a function of the unperturbed beam-beam strength.

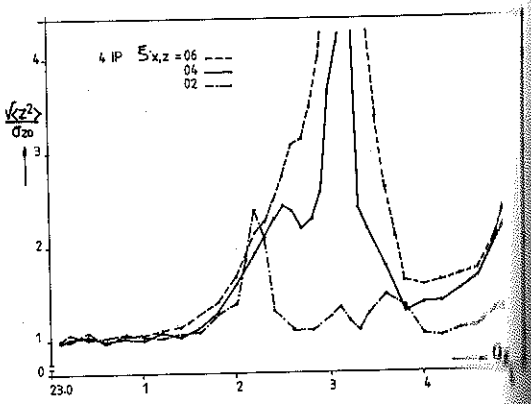

Fig. 14. Vertical blow-up against tune for different beam beam strengths (PETRA)

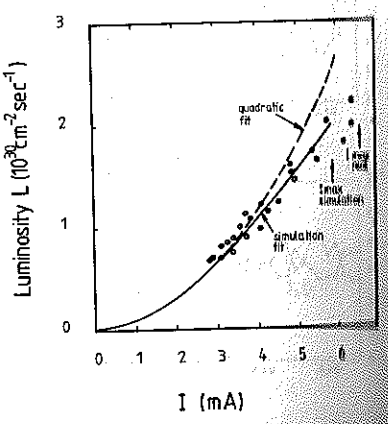

Fig. 15. Luminosity as a function of intensity (CESR)

It has been seen in the previous section that the maximum luminosity at a given beam current is strongly dependent on the tune values. It is also reasonable to expect that the optimum tune value will depend on the intensity level since this changes the total (perturbed) tune value and the tune spread.

The simulated variation of luminosity with unperturbed tune value for five different intensity levels is shown[14] for LEP in Fig. 12. It is somewhat surprising to find that each curve is somewhat similar in character and that an optimum tune value (Q_{yo} = 94.30) for one value of intensity is reasonably optimum for all intensities. Figure 13 shows how the relevant beam parameters vary with intensity [normalised to be the unperturbed beam-beam strength parameter (ξ_0)] for these fixed optimum tunes. The simulated behaviour is obviously similar to the experimental behaviour in that the luminosity increases initially quadratically and finally linearly with current. In addition it can be seen that the beam-beam strength parameter increases initially linearly and at high intensity saturates at a maximum value. This maximum value may be defined as the soft beam-beam limit (ξ). It can also be seen that the vertical beam size increases with intensity.

Figure 14 shows the simulated vertical blow-up factor in PETRA as a function of tune for different values of ξ. This plot is from weak-strong simulations without errors. Clearly there are ranges of tune values where there is no appreciable blow-up even at the highest value of ξ.

The simulated dependence of luminosity on beam intensity for CESR is shown in Fig. 15. Also shown on this plot is a quadratic fit to the experimental results. The simulation clearly gives good agreement with measurements.

4.3 Effect of the number of bunches

Changing the number of bunches causes changes in the following parameters:

i) the perturbed tune value via the total beam-beam tune shift, and of course the total beam-beam tune spread
ii) the betatron phase advance between IP's
iii) the superperiodicity of the accelerator and hence the numerology for systematic non-linear resonances
and iv) the number of beam-beam kicks per revolution (and hence per transverse damping time).

Since the first three of these phenomena are betatron-tune-dependent one should examine the dependence of the beam-beam effect on the number of bunches over a wide tune range.

Figure 16 shows for PETRA[12] the dependence of the vertical beam size on vertical tune for two interaction points. This plot may be compared with Fig. 14 which was performed for identical conditions except with four IP's. Clearly the blow-up factor is less with less bunches and the maximum blow-up occurs at a different tune value.

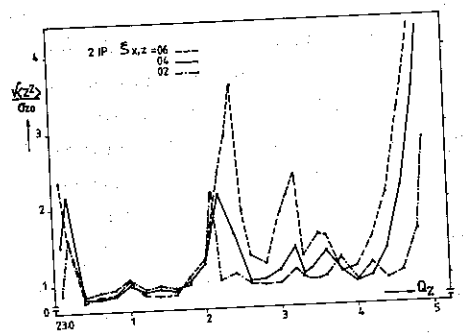

Fig. 16. Effect of number of bunches (PETRA).

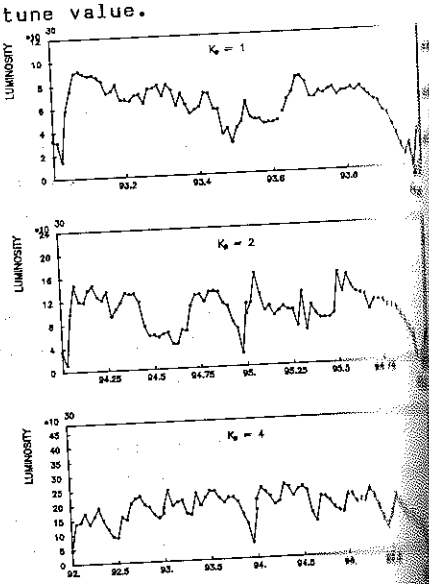

Fig. 17. Effect of number of bunches (LEP)

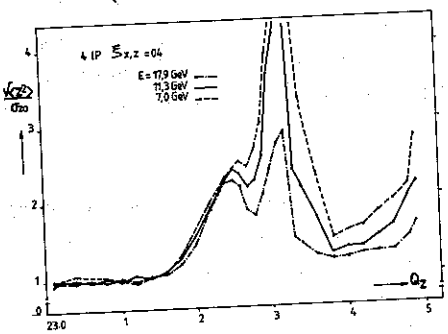

Fig. 18. Energy dependence (PETRA)

In Fig. 9 (for LEP) it was seen that the tune dependence repeats itself over an integer range modulo the number of bunches (i.e. every integer change in the Q advance per IP). Figure 17 shows the simulation results for LEP for one, two and four bunches over a tune range which corresponds to the non-integer range of 0.5 to 1.0 per IP. From these results it is clear also that the $\bar{\xi}$ (beam-beam limit) decreases with increasing number of bunches although the luminosity does increase with the number of bunches. It can also be seen from these plots that the tune dependence also varies with the number of bunches.

4.4 The energy dependence (transverse damping time)

In electron storage rings the transverse damping coefficient ($\alpha = 1/\tau$) is a strong function of the beam energy; e.g. in the absence of wiggler magnets α varies as E^3. Experimental evidence indicates that the beam-beam limit is a function of the transverse damping time.

Figure 18 shows the vertical blow-up factor as a function of vertical tune for three different energies in PETRA (weak-strong without errors). Clearly the blow-up is greater at lower energies.

Figure 19 shows the effect of variation of the transverse damping time for otherwise nominal LEP parameters at 22 GeV. For these runs the quantum excitation was also varied so as to maintain the beam size constant in all dimensions. It is clear from these plots that for all damping times greater than around 0.12 s the beam quality is totally unacceptable for physics. It should be noted that the damping times in LEP at 22 GeV are 0.80 and 0.32 s respectively without and with wiggler excitation. The behaviour in the plot of vertical blow-up shows that when τ_z becomes too large one of the beams becomes badly blown up whilst the other suffers no blow-up whatever. This situation (referred to as the beam flip-flop later) occurs when the beam-beam limit is grossly exceeded.

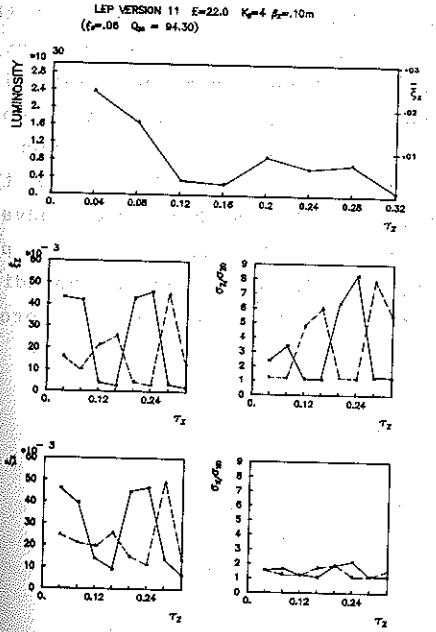

Fig. 19 Dependence on damping time (LEP).

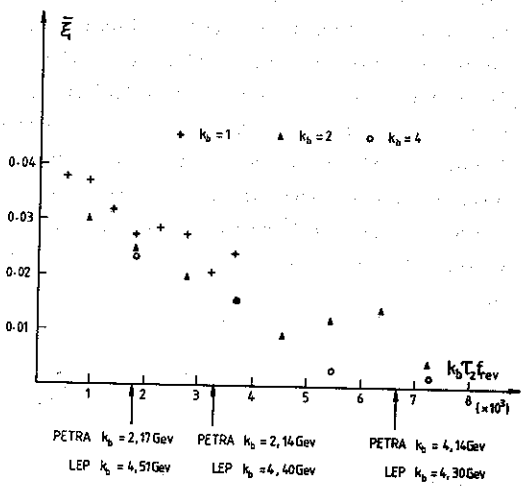

Fig. 20. Beam-beam limit as function of number of beam-beam kicks per transverse damping time.

Intuitively it appears more reasonable to define a parameter which relates the amount of damping between beam-beam collisions rather than the damping per revolution. In this case a reasonable parameter for comparing different machines could be the product of the number of interaction points, the vertical damping time and the revolution frequency. Figure 20 shows the beam-beam strength parameter ξ plotted as a function of $k_b \tau_z f_{rev}$ for the ensemble of LEP simulation results done at different bunch numbers. Also included along the x axis are indications of the value of $k_b \tau_z f_{rev}$ for various storage rings. From these results it appears that to have a reasonable beam-beam limit the number of beam-beam kicks per transverse damping time ($2k_b \tau_z f_{rev}$) should not exceed about 7000. In PETRA initial operation with four bunches at 14 GeV (giving around 13,500 beam-beam kicks per transverse damping time) was found to be extremely difficult due to the beam-beam effect. However operation with two bunches was highly successful. These observations together with those made at PEP suggest that this parameter is reasonable for comparison of the beam-beam effects in different storage rings.

4.5 The bunch length and β^* dependence

From equation (13) it appears that the luminosity increases linearly with the reciprocal of the vertical betatron amplitude function at the collision point provided the beam-beam limit is reached. However this simplified expression assumes a constant beam size along the interaction region. Equation (45) shows that the β^* (and hence the beam size) actually varies along the collision length. Since the collision length is given by the bunch length it is therefore necessary to include the bunch length in studying the effect of β^*. In addition to this 'static' effect there is also a modulation of the betatron phase advance between collision points. This effect is due to the differences in path lengths for particles of different energy and is described in Appendix 1 where it is shown that the amount of tune modulation (ΔQ_{mod}) is approximately given by

$$\Delta Q_{mod} \propto \frac{\sigma_s}{\beta^*} .$$

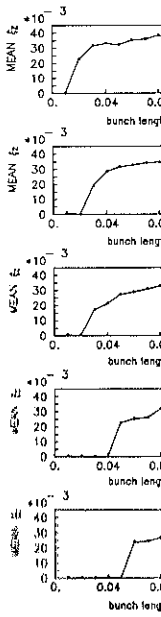

Figs. 21 and 22.

Figures 2
and luminosity
tio. It can b

i) For
leng

ii) Low
leng

iii) At v
indi
of t
tion
life
led
tabl
the
vers
in
inte

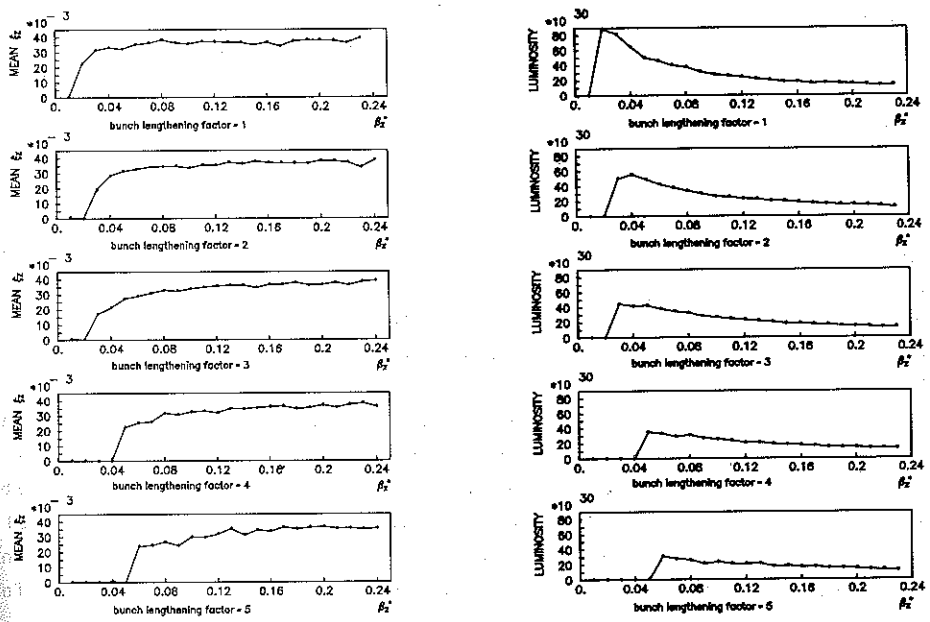

Figs. 21 and 22. Dependence on β_z^*/σ_s for LEP.

Figures 21 and 22 show the computed variation of the beam-beam limit and luminosity with the vertical β* value for various bunch lengths in LEP. It can be seen that

i) For large values of β_z^* the ξ is maximum and independent of bunch length

ii) Low β_z^* values give an increase in luminosity only when the bunch length is short compared to β_z^*.

iii) At very low values of β_z^* the lifetime becomes unacceptably low, indicated by $\bar{\xi} = 0$. For the simulation this happens when some of the superparticles are 'lost' against the aperture limitations. In reality this would incidate a very short quantum lifetime of several damping times or less. It should be pointed out here however that the lifetime is not necessarily acceptable for all cases where all superparticles are conserved. The lifetime may only be estimated by examination of the transverse charge distributions of the beams after the steady state in collision has been reached. Such distributions are shown later.

iv) A lower limit on the minimum value of β_z^*/σ_s appears to be in the range 1.5 to 2. This sets a limit to the minimum β_z^* in a given storage ring.

4.6 Effect of residual chromaticity

For large electron-positron storage rings, correction of the natural chromaticity is a major problem in itself. After correction the chromaticity (Q') is usually set slightly positive so as to stabilise head-tail modes. However during energy ramping the chromaticity is not controlled accurately and may therefore fluctuate both negatively and positively.

The dependences of the relevant machine parameters on the horizontal and vertical chromaticities are shown in Figs. 23 and 24 respectively for the LEP machine. It is apparent that the chromaticity has little influence on the beam-beam effect. (The maximum value of Q' = 20 is indeed large and unlikely to occur in a well-controlled storage ring.) This is not too surprising since it can be seen from Appendix 4 that for a β^*/σ_s of unity the equivalent chromaticity for LEP is around -50.

In fact for the conditions used in Figs. 23 and 24 the increase in chromaticity initially compensates the equivalent chromaticity due to the longitudinal modulation up to a value of around 5. For low values of β^*/σ_s it may be possible to increase the beam-beam limit by applying enough chromaticity so as to compensate for the 'equivalent chromaticity' due to the longitudinal modulation of the interaction point.

4.7 Machine errors

In section 4.5 the effect of modulation (at synchrotron frequency) of the phase advance between interaction points was described. The importance of this effect suggests that even static errors in the machine superperiodicity may be important. The main source of such asymmetries in phase advance is thought to be due to closed orbit distortions in sextupoles.

In Fig. 25 is shown the simulated dependence in PETRA[12] of the vertical blow-up factor as a function of tune without and with various degrees of horizontal phase advance errors between the interaction points. There is clearly a strong dependence on the strength of the horizontal phase advance error.

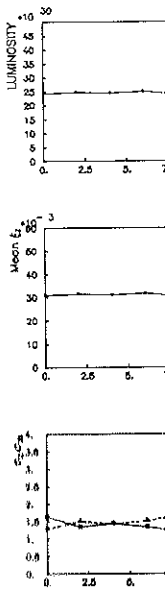

Figs. 23 and 24.

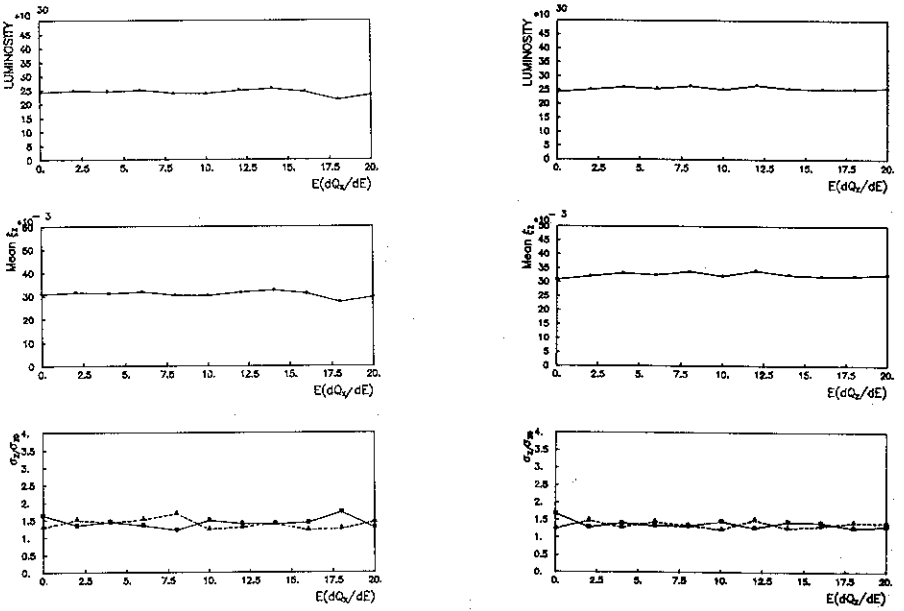

Figs. 23 and 24. Dependence on horizontal and vertical chromaticities.

Apart from the phase advance the other errors which have been included in simulations are:

i) the energy dispersion at the collision point
and ii) residual beam separations in the interaction points caused by the different closed orbits of the electrons and positrons.

These orbit differences have been shown to be significant in LEP and are produced by the fact that electrons and positrons may pass through the same sextupoles with different energies and hence different positions when the dispersion is finite.

Figures 26 and 27 show the effect on the vertical blow-up of phase advance errors and residual dispersions for the PETRA storage ring with only two interaction points.

In Fig. 28 the beam-beam limit is plotted as a function of the magnitude of each individual machine error. It is clear that all 'errors' significantly reduce the beam-beam limit. However, the beam-beam limit is seen to diminish rapidly for small values of the horizontal and vertical phase advance errors. Such small errors pose the greatest problem since they are difficult to measure with sufficient accuracy and therefore difficult to correct.

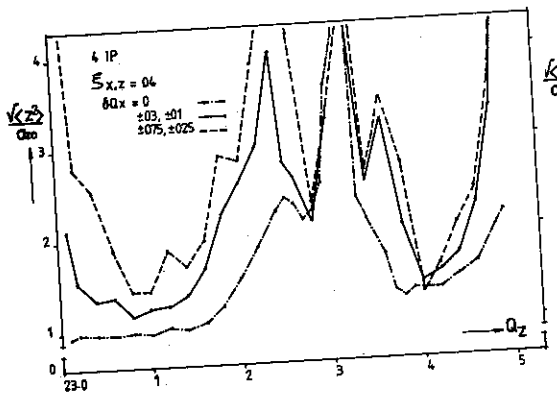

Fig. 25. Effect of phase advance errors (PETRA).

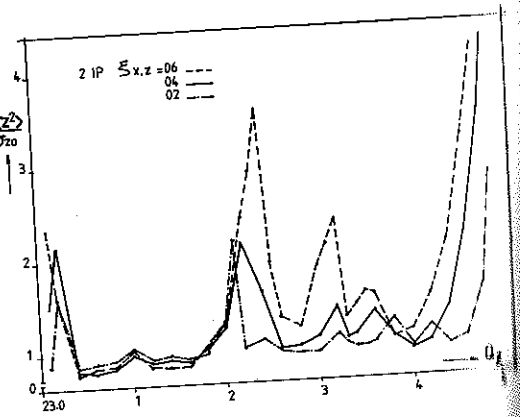

Fig. 26. No errors (PETRA).

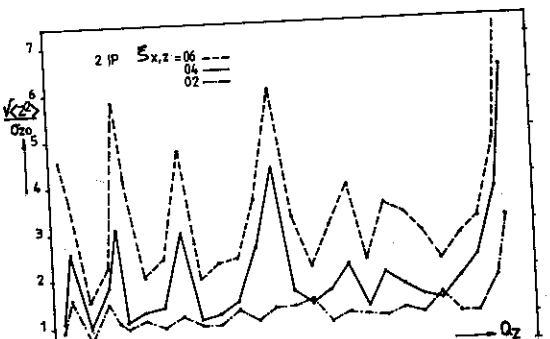

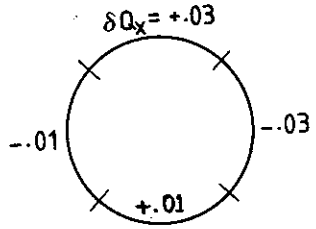

Fig. 27. Phase advance plus dispersion errors. ($\delta Q_{x,z}$ = ±0.02, D_{xo} = ±11 cm)

5. ASYMMETRIC BEAM-BEAM STRENGTHS

In a real storage ring with many circulating bunches it is often unavoidable that the bunches or even the beam may have different intensities. In this section an investigation is made of the beam-beam effects when the beams have different intensities. Two situations were chosen (and simulated for LEP):

i) one beam of constant high intensity and the intensity of the other beam varied over a range,

and ii) one beam with constant low intensity and the intensity of the other beam varied over a range: this is the 'weak-strong' case.

5.1 Constant high-intensity beam against variable intensity

In this section the intensity of one beam (beam B) was fixed so as to produce a beam-beam strength parameter (ξ) of 0.06 (6.6 mA) and the intensity of the other beam (A) was varied over an ξ range of zero to around 0.08 (9.0 mA).

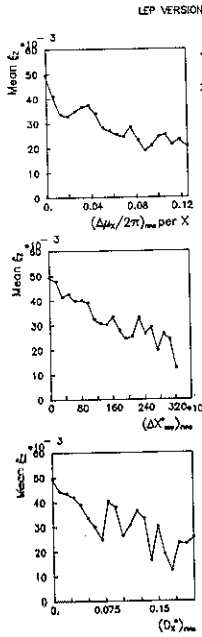

Fig. 28. Effect

Figure 29 sho
and the vertical t
beam A. It is c
stronger beam cau
during even more t
the stronger beam
weaker beam is in
and that of the s
approximately equ
This is a sort of
in fig. 29 that f
the equilibrium p
situation. This
extensively16).

It is also in
which exist in th
logarithmic scale
first case. In
intensity beam are
and are shown on
the elastic cases

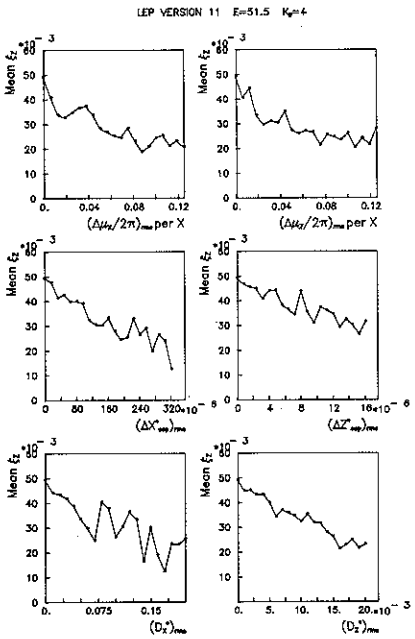

Fig. 28. Effect of errors (LEP).

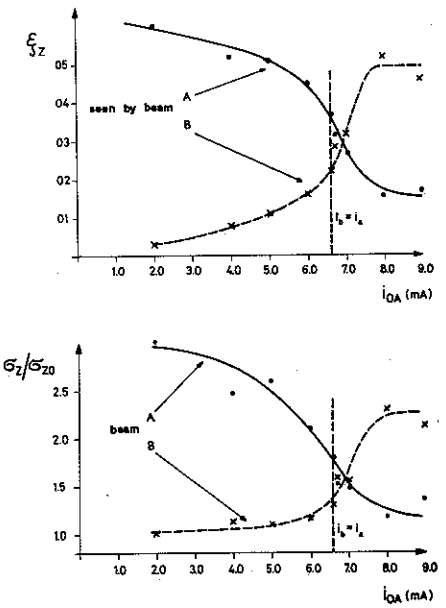

Fig. 29. Asymmetric beams (LEP).

Figure 29 shows the beam-beam strength parameters seen by each beam and the vertical blow-up factor plotted as a function of the intensity of beam A. It is clear that, at large differences in beam intensities, the stronger beam causes significant blow-up in the weaker beam thereby reducing even more the beam-beam strength. Consequently in this situation the stronger beam suffers practically no blow-up. As the strength of the weaker beam is increased its vertical blow-up factor starts to decrease and that of the stronger beam starts to increase. When both beams have approximately equal intensities their vertical dimensions become equal. This is a sort of beam-beam equilibrium. It is clear from the behaviour in Fig. 29 that fairly small variations of the beam-beam strength around the equilibrium point can cause the beams to flip into a weak-strong situation. This flip-flop has been experimentally observed and studied extensively[16].

It is also interesting to examine the transverse charge distributions which exist in the flip-flop situation. Figures 30 and 31 show (on a logarithmic scale) the vertical distributions and Fig. 32 shows the horizontal case. In all these plots the charge distributions of the constant intensity beam are shown on the right while those of the varying intensity beam are shown on the left. From Fig. 30 it is clear that in the highly asymmetric cases the weak beam becomes badly blown up and the tails become

non-Gaussian. Such long tails of course drastically reduce the quantum lifetime and are the cause of the intensity limitation produced by the beam-beam effect.

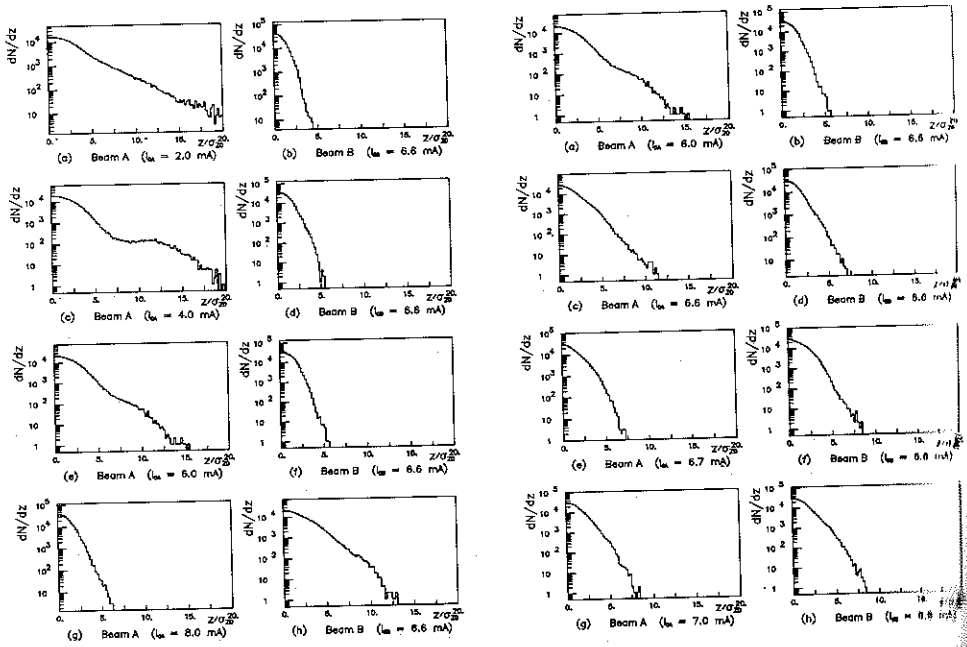

Figs. 30 and 31. Vertical charge distributions with asymmetric beams (LEP).

Figure 31 shows how the vertical distribution changes with rather small variations around the equilibrium intensity. It can be seen that at equilibrium (with $\xi \simeq 0.03$) both beams are slightly enlarged but the distributions remain reasonably Gaussian [Fig. 31 (e) and (f)]. However a small imbalance of around 1.5% from the equilibrium situation causes a large increase in the density in the tails of the weaker beam [Fig. 31 (c)].

These results highlight the importance of balancing the beam-beam strengths of each beam. It should be remembered that the beam-beam strength is a function not only of the intensity but also β^*, the beam energy, and the beam cross-section. Any phenomena which can cause differences in any of these parameters can cause an imbalance and hence a lower beam-beam limit.

Figure 32 shows that the horizontal charge density in the 'tails' is less than Gaussian. This seems to indicate a transverse energy cooling at large betatron amplitudes.

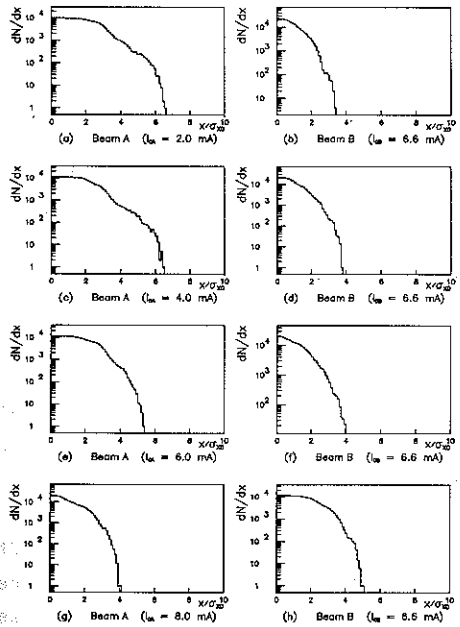

Fig. 32. Horizontal charge distribution with asymmetric beams (LEP).

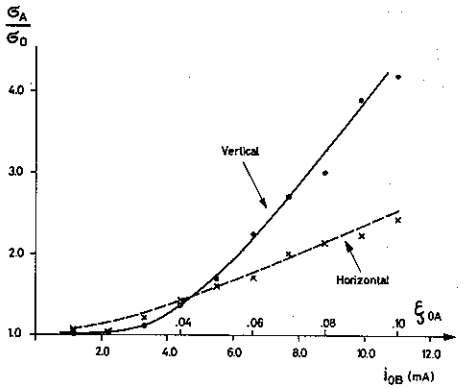

Fig. 33. Weak-strong (LEP).

5.2 Constant low-intensity beam against variable intensity

In this case the intensity of one beam (beam A) is fixed at vanishing intensity and that of the other (beam B) is varied over a wide range (ξ_0 varied from 0.01 to 0.10). Figure 33 shows the transverse blow-up of the

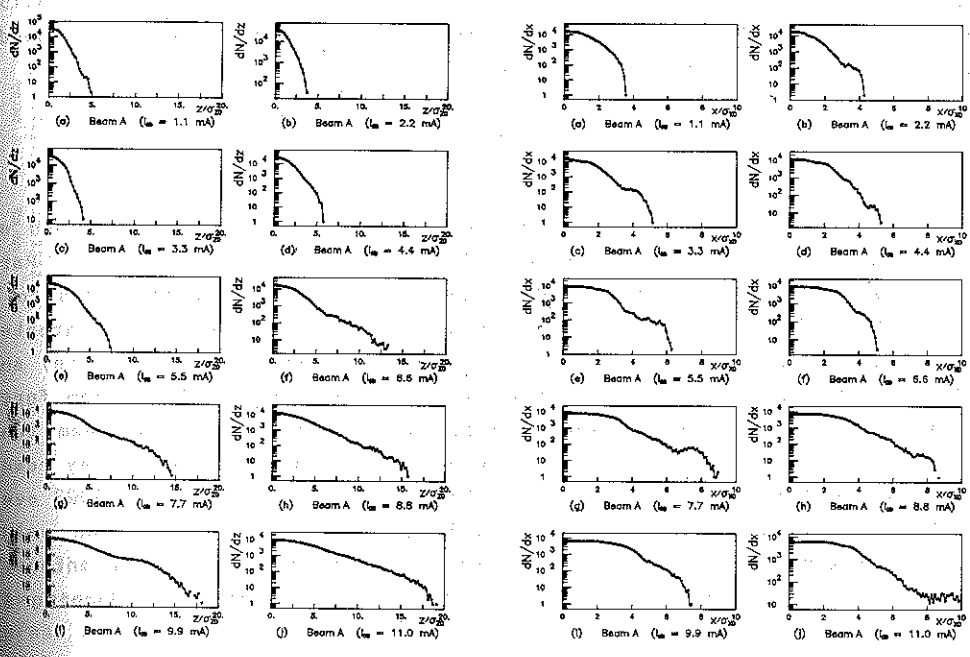

Figs. 34 and 35. Vertical and horizontal charge distributions for weak-strong (LEP).

weak beam as a function of the beam-beam strength of the strong beam. In the vertical plane there is practically no blow-up until the strength of the strong beam is increased beyond $\xi_0 > 0.03$. Above this value the blow-up increases rather rapidly with increasing ξ_0. In the horizontal plane the blow-up is significantly less.

Figures 34 and 35 show the corresponding vertical and horizontal charge distributions. Vertically the tails of the distribution start to become non-Gaussian at ξ_0 values greater than around 0.05 (i.e. 5.5 mA). For very large intensities the vertical charge distribution becomes almost exponential in the tails.

In the horizontal plane (Fig. 35) the tails do become enlarged but to a much lesser extent than in the vertical plane (note the difference in the horizontal scale between Figs. 34 and 35).

As described previously the beam-beam force produces a tune shift which decreases with increasing betatron amplitude. It is therefore interesting to examine the beam-beam tune shift distribution. This is plotted in Fig. 36 again for the weak-strong situation. Low intensities [plots (a) and (b)] produce a reasonably regular distribution with a total tune spread corresponding to approximately the product of the number of interaction points and the beam-beam tune shift per interaction point. However as the beam-beam strength is increased the tune distribution becomes less regular. From plots (d), (e) and (f) it appears that the distribution density reduces abruptly for ΔQ_{bb} values greater than 0.19. Since the value of the unperturbed vertical tune is 94.35 this corresponds to a perturbed vertical tune value of

$$Q_y = 94.50 \quad .$$

The strange behaviour of the distribution may then be explained at least qualitatively by the presence of the half integer resonance. Particles which have initially small betatron amplitudes are subjected to a large beam-beam tune shift and have perturbed tune values much greater than 94.50, i.e. they reside to the right-hand side of plots (d), (e) and (f). Under the influence of quantum excitation and the beam-beam force these particles diffuse towards larger amplitudes (lower beam-beam tune shifts), i.e. they move from right to left in the plots. When they reach the half integer resonance their growth rate increases and they move even faster to the left. As their amplitude increases their tune value decreases and they finally escape from the stopband of the half integer. The particles now have large amplitudes and the synchrotron damping is

stronger than the
towards smaller am
the plots. Howev
driven towards lar
cally at least) pa
in these plots.
to the left of the
hypothesised mecha
value and the tota
mining the beam-be

It has alread
dent on the unpert
the number of bun
produce higher bea

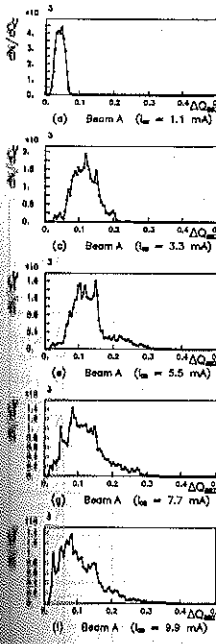

Figs. 36. Tune d
weak-s

5. COMPENSATION

The simulatio
the beam-beam lim
spread as well as

stronger than the quantum excitation. Hence the particles tend to damp towards smaller amplitudes (larger tunes), i.e move from left to right in the plots. However when they reach the half integer they are once again driven towards larger amplitudes. It therefore appears that (statistically at least) particles only cross the half integer from right to left in these plots. This of course causes a build-up of distribution density to the left of the half integer. It is important to realise that if this hypothesised mechanism is correct, it is clear that the unperturbed tune value and the total beam-beam tune spread are important factors in determining the beam-beam limit.

It has already been seen that the beam-beam limit is in fact dependent on the unperturbed tune. In addition the evidence from variation of the number of bunches indicates that lower total beam-beam tune spreads produce higher beam-beam limits.

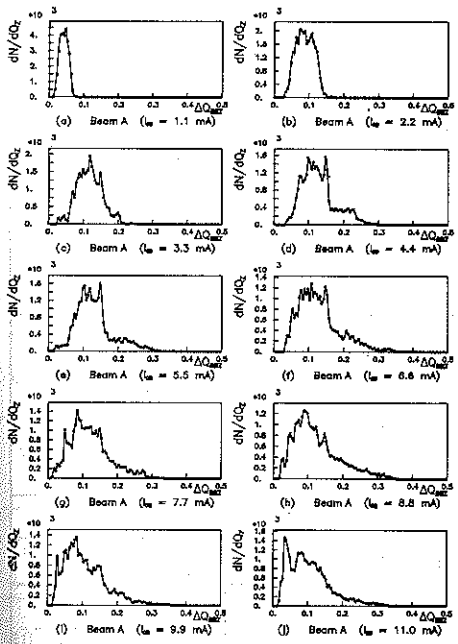

Figs. 36. Tune distributions for weak-strong (LEP).

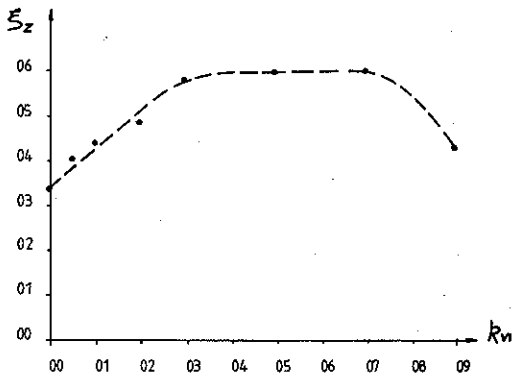

Fig. 37. Beam-beam limit with compensation of the tune dependence on amplitude.

6. COMPENSATION OF THE BEAM-BEAM TUNE DEPENDENCE ON AMPLITUDE

The simulation results presented in the previous section suggest that the beam-beam limit is determined to some extent by the beam-beam tune spread as well as the unperturbed tune value. If this is true it should

therefore be possible to increase the beam-beam limit by partial (or full) compensation of the tune spread. In a real storage ring, tune dependence on betatron amplitude could be implemented by octupoles. In the computer code this can be simulated by making the phase advance (of each superparticle) in the machine lattice dependent on the invariant betatron amplitude. The parameters for the compensation were chosen as follows:

$$\Delta Q_{comp} = - k_1 N_x \xi_0 \left(1 - \left(\frac{A}{k_2 A_0} \right)^2 \right) \qquad (48)$$

where N_x is the number of interaction points

$A_1 A_0$ are the betatron invariants of the superparticle and a particle at one σ respectively

k_1 determines the fraction of the quadrupolar shift

and k_2 determines the number of σ at which the compensation passes through zero initially.

Table 1.

Dependence of $\bar{\xi}_z$ on K_1

Row No.	K_{v1}	ξ_0	$\bar{\xi}_z$	ξ_x	ξ_z	$\frac{\sigma_x}{\sigma_{x0}}$	$\frac{\sigma_z}{\sigma_{z0}}$	Beam
1	0.0	0.09	.034	.053 / .028	.049 / .025	1.79 / 1.31	1.99 / 1.40	A / B
2	0.05	0.09	.041	.039 / .038	.041 / .041	1.55 / 1.53	1.43 / 1.46	A / B
3	0.10	0.09	.044	.042 / .038	.042 / .050	1.56 / 1.47	1.18 / 1.45	A / B
4	0.20	0.09	.049	.045 / .033	.061 / .040	1.67 / 1.44	1.28 / 1.05	A / B
5	0.30	0.09	.058	.040 / .039	.062 / .055	1.55 / 1.53	1.08 / 0.97	A / B
6	0.50	0.09	.060	.034 / .042	.051 / .076	1.50 / 1.64	0.92 / 1.10	A / B
7	0.70	0.09	.060	.033 / .044	.054 / .071	1.45 / 1.68	0.90 / 1.02	A / B
8	0.90	0.09	.043	.054 / .026	.057 / .036	1.90 / 1.30	1.35 / 1.22	A / B

Compensation was initially applied in the vertical plane only (subscripts v). An optimum value for the vertical factor k_{v2} was found (by trial and error) to be around 4.0. The unperturbed beam-beam tune shift was set at 0.09. Figure 37 and Table 1 show the dependence of the beam-beam limit and the vertical blow-up factor on the vertical factor k_{v1}. Clearly the beam-beam limit is increased by compensating the vertical beam-beam tune spread. The broad maximum in ξ_y occurs around $k_{v1} = 0.5$. It is also evident that for values of k_{v1} between 0.3 and 0.7 there is no measurable blow-up in the vertical beam size. The reduction in the ξ_0 from 0.09 to around 0.06 is caused by horizontal blow-up. This can be seen from Table 1 which gives the details of Fig. 37.

Since in Fig. 37 there is no vertical blow-up, it is clear that the beam-beam limit has not yet been reached. The optimum compensation values ($k_{v1} = 0.5$ and $k_{v2} = 4.0$) were then fixed and ξ_0 was increased. The results are shown in Table 2 where a maximum beam-beam tune shift of 0.069 is reached; nearly twice the uncompensated value. However it is again interesting to note that even at $\xi_z = 0.069$ there is no vertical blow-up; the limit is again set by horizontal blow-up.

Table 2.

Dependence of $\bar{\xi}_z$ on ξ_0

Row No.	K_{v1}	ξ_0	$\bar{\xi}_z$	ξ_x	ξ_z	$\frac{\sigma_x}{\sigma_{x0}}$	$\frac{\sigma_z}{\sigma_{z0}}$	Beam
9	0.50	0.06	0.044	0.039	0.053	1.41	1.10	A
				0.031	0.040	1.25	0.93	B
6	0.50	0.09	0.060	0.034	0.051	1.50	0.92	A
				0.042	0.076	1.64	1.10	B
10	0.50	0.12	0.069	0.034	0.062	1.63	0.91	A
				0.047	0.0850	1.89	1.05	B
11	0.50	0.15	0.057	0.035	0.049	1.80	1.13	A
				0.046	0.073	2.07	2.45	B

Several attempts were then made to combine horizontal and vertical compensation. However in all cases the addition of the horizontal compensation deteriorated the improvement given by vertical compensation alone. This is not yet properly understood but may be due to the fact that the compensating quadratic tune dependence on betatron amplitude is a good approximation in the vertical plane but less good in the horizontal plane for the ribbon-shaped LEP beams.

It is worthwhile to point out here that these tests of tune spread compensation were performed solely to examine the effect on the beam-beam limit. Of course the inclusion of such a strong tune dependence on amplitude in an accelerator lattice also requires close examination from the point of view of single-beam dynamics. In addition, for LEP the required tune dependence on amplitude found from these results would necessitate several hundred metres of magnetic octupoles.

7. BEAM-BEAM EFFECTS DURING ACCUMULATION AND ACCELERATION

For modern electron-positron storage rings where the horizontal dimensions are much larger than the vertical (i.e. $\sigma_x^* \gg \sigma_y^*$) the beam-beam tune shifts are approximated by [from equations (8) and (9)]

$$\xi_{x_0} = \frac{r_e\, i_b\, \beta_x^*}{2\pi e f_{rev}\, \gamma\, \sigma_x^{*\,2}} \quad ; \quad \xi_{y_0} = \frac{r_e\, i_b\, \beta_y^*}{2\pi e f_{rev}\, \gamma\, \sigma_x^* \sigma_y^*} \,. \tag{49}$$

In the absence of wiggler magnets and when β^* is constant with energy, both σ_x^* and σ_y^* are directly proportional to energy. Hence

$$\xi_{x,y} \propto \frac{i_b}{\gamma^3} \,. \tag{50}$$

Clearly if the beam-beam limit is to be reached at a certain current at design energy it would be greatly exceeded for the same current at injection energy. For this reason the beams are separated in the interaction regions during accumulation and acceleration.

For beams separated by an amount (δ) large compared to the transverse beam dimensions

$$\xi_{xs} = \frac{r_e\, i_b}{2\pi e f_{rev}\, \gamma}\,\frac{\beta_x^*}{\delta^2} \quad ; \quad \xi_{ys} = \frac{r_e\, i_b}{2\pi e f_{rev}\, \gamma}\,\frac{\beta_y^*}{\delta^2} \; . \tag{51}$$

If the separations are measured in the number of σ_x^* (i.e. $\delta = k_x \sigma_x^*$):

$$\xi_{xs} = \frac{\xi_{x_0}}{k_x^2} \quad ; \quad \xi_{ys} = \frac{\xi_{y_0} k_c}{k_x^2} \tag{52}$$

where $k_c = \dfrac{\sigma_y^*}{\sigma_x^*} \ll 1$.

Equation (52) indicates that for 'optimum' coupling ($\xi_{x_0} = \xi_y$) and large separations

$$\xi_{ys} = k_c \xi_{xs} \; . \tag{53}$$

It is also clear that the high values of ξ_0 at injection can be reduced to the appropriate amount either by horizontal or vertical separations.

The LEP simulation code was used to investigate the beam-beam effect during the following modes of a storage ring cycle.

i) Injection and accumulation. Injection was simulated in the horizontal plane so as to facilitate synchrotron[17] or betatron accumulation or a combination of the two.

ii) Static separations of the accumulated beams after accumulation. This is the situation just before energy ramping.

iii) Static separations at design energy.

iv) Bringing the beams into collision at design energy.

4.1 Injection and accumulation

Figure 38 shows[18] the time evolution of the beam sizes (normalised to the steady state beam sizes) for different values of horizontal separation. In plot (a) it can be seen that with a horizontal separation of $10\sigma_x$ the injected beam converges towards its equilibrium size (1.0) in both planes with approximately the correct damping rate (τ = 0.4 s). The initial fast 'blow-up' in the horizontal plane is caused by filamentation due to the tune dependence on amplitude produced by the residual beam-beam forces.

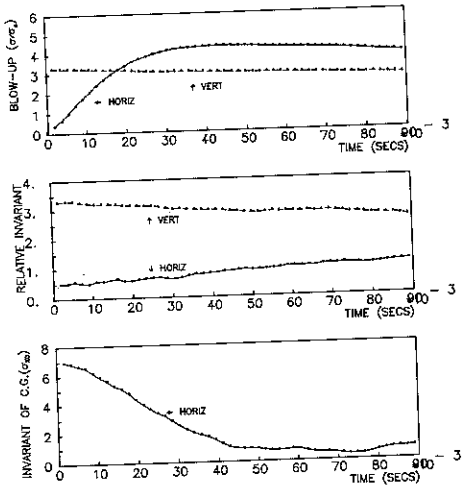

Fig. 38(a). Horizontal separations of $10\sigma_x$ (LEP)

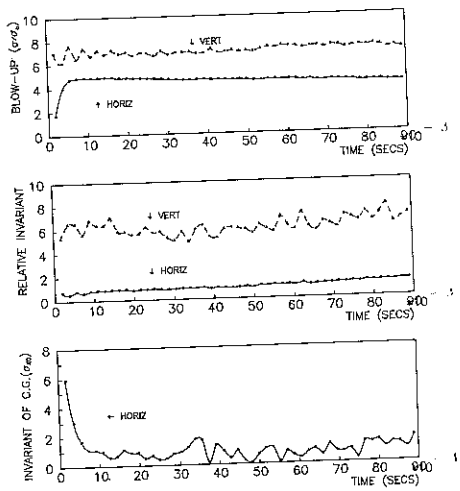

Fig. 38(b). Horizontal separations of $7\sigma_x$ (LEP).

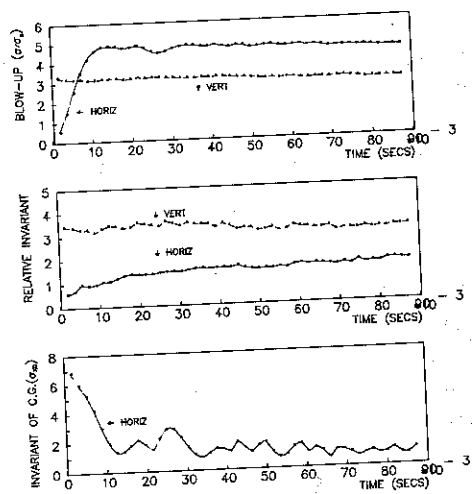

Fig. 39(a). Vertical separations of $20\sigma_y \equiv 1.25\sigma_x$ (LEP).

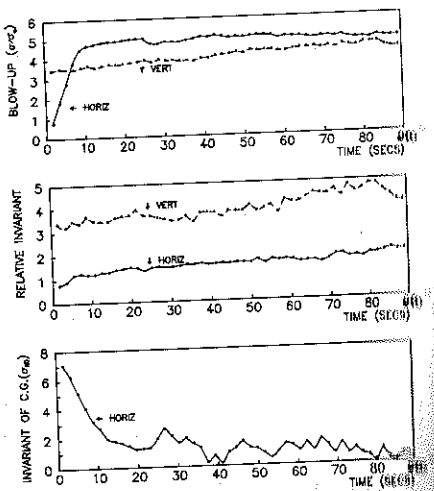

Fig. 39(b). Vertical separations of $10\sigma_y \equiv 0.62\sigma_x$ (LEP).

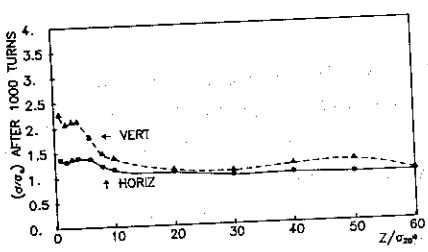

Fig. 40. Static separations at 20 GeV (LEP).

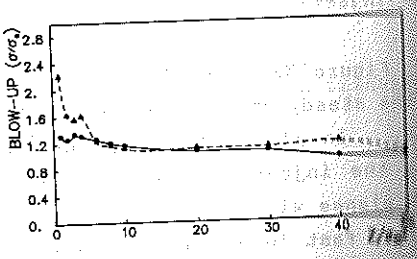

Fig. 41. Static separations at 51.5 GeV (LEP).

In plot (b) the horizontal separations are reduced to $7\sigma_x$; these results show that excessive vertical blow-up occurs which would prevent efficient injection.

Figure 39 shows the simulation results for vertical separations. It is apparent that vertical separations of $20\sigma_y$ (corresponding to $1.25\sigma_x$ are perfectly adequate to allow efficient injection to LEP at the maximum intensity which corresponds to $\xi_0 = 0.06$. These results clearly indicate that vertical separations are to be preferred.

7.2 Static separations at injection and design energy

In this case the two separated intense counter-rotating beams experience each other's residual beam-beam forces. Figures 40 and 41 show the computed relative blow-up as a function of the vertical separation at injection energy and design energy.

These results indicate that even small vertical separations do not have a disastrous effect on the beam size. However it should be remembered that the conditions here involve using wiggler magnets at injection energy. These wigglers increase the transverse emittances so that the unperturbed beam-beam strength is only around 0.06. In the absence of wigglers (as is the case for existing storage rings) ξ_0 would be of the order of unity and of course small separations would indeed have disastrous consequences.

Similar results for horizontal separations[18] show large beam-beam blow-up at around $2\sigma_x^*$ separation.

7.3 Bringing the beams into collision at design energy

In the previous section, the simulation results showed that static vertical separations of any amount do not cause excessive blow-up when the ξ_0 is around 0.06. It follows that bringing the beams slowly into collision will have no detrimental effect. This was confirmed by reducing the separations exponentially with a time constant of 0.25 s.

Figure 42 shows the vertical blow-up as the beams are brought into collision horizontally with different time constants. In order to avoid excessive blow-up a time constant of 0.5 ms (five turns in LEP) is required.

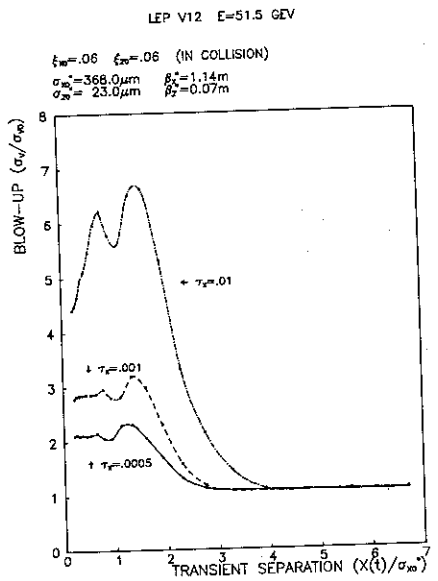

Fig. 42. Bring beams into collision horizontally with varying time constants.

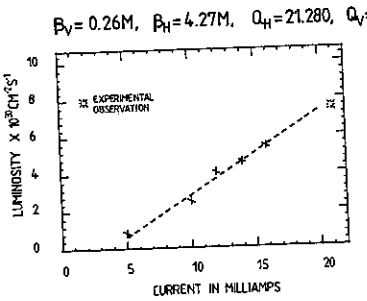

Fig. 43. Luminosity against current (PEP1).

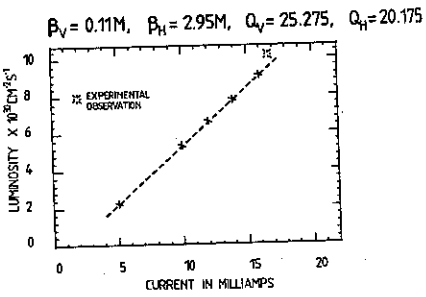

Fig. 44. Luminosity against current (PEP2).

8. COMPARISON OF EXPERIMENTAL AND SIMULATION RESULTS

It is rather surprising to find that although an enormous amount of work has been published on simulation of the beam-beam effect, very little work has actually been published on systematic comparisons of simulation results with experimental measurements. Simulation sceptics would say that this work has of course been done but the results were not in good agreement with each other and were therefore not published. However the problem is somewhat more complicated. Normally a simulation code is specifically written to examine the beam-beam effect. In a real storage ring the interaction of all possible effects may greatly complicate the interpretation of the results. Take as a simpler example the dependence on machine tune. A simulation program may predict that the luminosity in collision is improved by changing the machine tune. However the proposed new tune value may be unacceptable for beams not in collision due to single-beam effects such as synchro-betatron resonances. Hence it is extremely important when comparing experimental and simulation results over a range of parameters that the implication of the parameter change is well understood in the absence of the beam-beam effect. Or even better

the simulation should include all known effects, even the single-beam ones, with suitable in-built diagnostics to identify the source of the effect.

8.1 PETRA

A detailed study of the beam-beam effect in PETRA has been performed[12]. The following parameters have been varied for the weak-strong case.

i) **The machine tune.** Both the integer and non-integer part of the machine tune were varied and the experimental behaviour agreed qualitatively with the simulation predictions.

ii) **Short and long straight sections.** The effect of colliding in high β^* and low β^* interaction regions was observed. It was found that provided the ratio β_y^*/β_x^* was held constant there was no significant influence. The computer simulation had predicted this.

iii) **Number of interaction points.** The vertical blow-up was found to be worse as the number of interaction points was increased. This was in qualitative agreement with simulation results.

iv) **Dispersion at the interaction points.** The observed vertical blow-up was found to become reduced when the horizontal dispersion at the interaction point was reduced. This was predicted by the simulation.

v) **Small beam separations.** It was found experimentally that small separations of the beams in the interaction points did not cause a large increase in the vertical blow-up factor. Again this agreed with the computer simulation results.

8.2 CESR

As far as I know there is only one published comparison between simulation and experimental results for CESR. These results have already been shown in Fig. 10 and do indeed show good agreement in the shape of luminosity against current. The absolute level was adjusted by a fitting parameter.

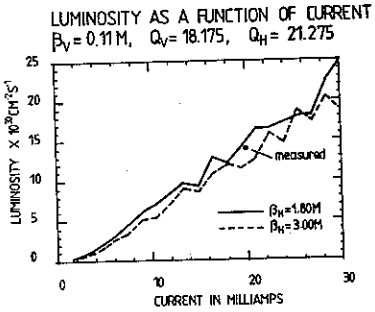

Fig. 45. Luminosity as a function of current (PEP3).

8.3 PEP

The LEP simulation program was used to simulate[19] the beam-beam effect in PEP with two main intentions. Firstly to test the validity of the program by comparison with experimental data from previous PEP runs, and secondly, to search for an improvement in the operating conditions of PEP. A successful prediction would obviously also enhance the credibility of the program.

Two older versions of PEP were firstly simulated (PEP1 and PEP2). The input rms values of the machine errors wer based on actual production runs in PEP. Figures 43 and 44 show the simulated results of luminosity against current for the initial medium β^* version (PEP1) and the low β^* version (PEP2). The linear dependence above 5 mA per beam is routinely observed in PEP under practically all operating conditions. The maximum luminosities achieved in these two configurations are indicated by asterisks on the graphs. Clearly the simulation is in excellent agreement with the measured luminosities. In addition the vertical blow-up was reported to be in good agreement with measurements from the synchrotron light monitors.

The simulation was then used to search for a new operation condition. The search predicted that the luminosity (and the beam-beam limit) would be increased by around 40% by operating at integer tunes of Q_y above 18 and Q_x above 21 (see Fig. 45). Several months later PEP was switched on with these new tune values. The measured luminosity is plotted as an asterisk in Fig. 45. The agreement is evident.

Subsequent routine operation of PEP increased the beam-beam limit from this value (0.035) to 0.05. This improvement was achieved interactively by the operators by[20]

i) 'tweaking' the closed orbit to find the 'golden orbit'

ii) using a
tion of
city.

It is consi
fact producing a
the beam-beam limi

ii) using a different sextupole correction which allowed modification of the sextupole correction without affecting the chromaticity.

It is considered likely[20] that both these manipulations are in fact producing a reduction in the machine errors and thereby increasing the beam-beam limit as predicted in the simulation code.

APPENDIX 1

RELATIONSHIP BETWEEN THE NON-LINEAR TERMS OF THE BEAM-BEAM KICK AND THE LINEAR STRENGTH PARAMETER ξ

Let us define

$$\xi_{tot} = -\frac{\beta}{4\pi}\frac{\Delta r'}{r}$$

as the total beam-beam strength parameter, not limited to the linear case of r small.

For a beam with circular cross-section and Gaussian charge distribution the volume charge density is

$$\rho = \frac{Ne_1}{(2\pi)^{\frac{3}{2}}\sigma_r^2\sigma_s}\exp\left\{-\frac{r^2}{2\sigma_r^2}-\frac{s^2}{2\sigma_s^2}\right\} \qquad (A1)$$

where Ne_1 is the total bunch charge
σ_r is the rms radius
σ_s is the rms bunch length

Solving Maxwell's equation ($\nabla\cdot E = \frac{\rho}{\varepsilon_0}$) in cylindrical co-ordinates, i.e. assuming $E_s = 0$,

$$\frac{1}{r}\frac{\partial(rE_r)}{\partial r} = \frac{\rho}{\varepsilon_0}$$

gives

$$E_r = \frac{Ne_1}{(2\pi)^{\frac{3}{2}}\sigma_r^2\sigma_s}\exp\left(-\frac{s^2}{2\sigma_s^2}\right)\left[1-\exp-\frac{r^2}{2\sigma_r^2}\right]. \qquad (A2)$$

The change in radial momentum is

$$\Delta(P_T) = \Delta\left(\gamma m_0 c \frac{dr}{ds}\right) = \int_{-\infty}^{\infty} F_r dt \qquad (A3)$$

where F_r is the radial force $= e_2(E_r + vxB)$
$\simeq 2e_2E_r$ for relativistic particles ($v = c$).

In (A3) $t = \frac{s}{2c}$ since both beams are travelling with $v = c$,

$$\Delta\left(\gamma m_0 c \frac{dr}{ds}\right) = \frac{1}{c} \int_{-\infty}^{\infty} e_2 E_r ds$$

$$\Delta r' = \frac{e_2}{\gamma m_0 c^2} \int_{-\infty}^{\infty} E_r ds \quad . \qquad (A4)$$

Substituting E_r from (A2) gives

$$\Delta r' = \frac{N e_1 e_2}{2\pi\gamma m_0 c^2 \varepsilon_0 r} \left[1 - \exp \frac{-r^2}{2\sigma_r^2}\right] \qquad (A5)$$

(for beams of opposite charge $e_1e_2 = -e^2$).

Using $r_e = \frac{e^2}{4\pi\varepsilon_0 m_0 c^2}$ gives for beams of opposite charge

$$\frac{\Delta r'}{r} = -\frac{2Nr_e}{\gamma r^2} \left[1 - \exp \frac{-r^2}{2\sigma_r^2}\right] \qquad (A6)$$

and expanding the exponential

$$\frac{\Delta r'}{r} = -\frac{Nr_e}{\gamma\sigma_r^2} \left[1 - \frac{1}{2!2}\left(\frac{r}{\sigma_r}\right)^2 + \frac{1}{3!2}\left(\frac{r}{\sigma_r}\right)^3 \ldots\ldots\right] \qquad (A7)$$

and for $r \ll \sigma_r$

$$\xi_{tot} = \xi_{linear} = \frac{N r_e}{4\pi\gamma} \frac{\beta}{\sigma_r^2} \cdot \qquad (A8)$$

Hence in general

$$\xi_{tot} = \xi_{linear} \left[1 - \frac{1}{2!2} \left(\frac{r}{\sigma_r}\right)^2 + \frac{1}{3!2^2} \left(\frac{r}{\sigma_r}\right)^3 \cdots\cdots \right] . \qquad (A9)$$

↑ octupole coefficient

↑ 12-pole coefficient

Equation (A9) indicates that as the relative displacement increases more and more higher-order terms are needed to describe the beam-beam force for a round Gaussian beam.

APPENDIX 2

SIMULATION OF TRANSVERSE DAMPING

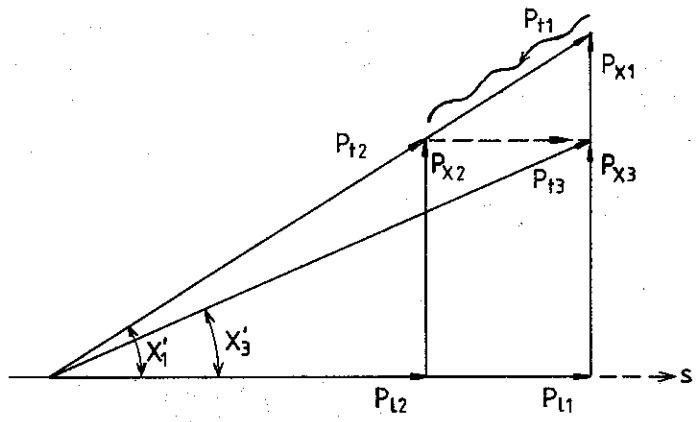

The subscripts 1, 2, 3 refer to before emission of any quanta in the arcs, after emission of all quanta, and after acceleration in the cavities, respectively.

On traversal of the arc the total momentum p_{t1} is reduced to P_{t2} due to synchrotron radiation where

$$P_{t1} = m_1 v_1 \quad ; \quad P_{x1} = m_1 v_1 x_1' = P_{t1}\, x_1'$$

and

$$P_{t2} = m_2 v_2 \quad ; \quad P_{x2} = m_2 v_2 x_2' = P_{t2}\, x_2' \ .$$

From the diagram clearly $x_1' = x_2' = x'$. Consequently there is no transverse damping in the arcs when working in the co-ordinates x, x'. However working in momenta,

$$\Delta P_x = P_{x1} - P_{x2} = x'(P_{t1} - P_{t2}) \ .$$

Hence

$$\Delta p_x \simeq p_{x1} \frac{\Delta p_t}{p_{t1}} . \qquad (A2.1)$$

Clearly equation (A2.1) provides damping, provided $< \frac{\Delta p_t}{p_{t1}} >$ is less than zero. It follows that the transverse damping can be simulated in the arcs by using equation (A2.1) and working in units of momentum. It is equally clear that since $x_1' = x_2'$ damping in this co-ordinate system does not occur in the arcs. However after traversal of an RF cavity

$$p_{x3} = p_{x2} \quad \text{(i.e. no damping in } p_x\text{)}.$$

Therefore $p_{t3}x_3' = p_{t2}x_2'$

and with

$$\Delta x' = x_2' - x_3' = x_2'\left(\frac{p_{t3}-p_{t2}}{p_{t3}}\right) .$$

Thus

$$\Delta x' = x_2' \frac{\Delta p_t}{p_t} . \qquad (A2.2)$$

It is clear that in the co-ordinate system x, x' the damping occurs on traversal of the cavity. In both (A2.1) and (A2.2)

$$\frac{\Delta p_t}{p_t} \simeq \frac{\Delta E_{RF}}{p_t} \quad \text{since} \quad p_x \ll p_t .$$

APPENDIX 3

EFFECTS INCLUDED IN RECENT SIMULATION CODES (e^+e^-)

The following gives a list of the salient effects (as published included in the recent simulation codes. The properties of the codes are those used in the published results.

(a) LEP 1

Included:

i) Truly strong-strong
The calculated root mean square values of the beam dimensions are used to define the sigma of the assumed Gaussian charge distribution and thereby the beam-beam force for each beam. This can be done on every beam-beam collision or less if required.

ii) Six-dimensional phase space

iii) Quantum excitation and damping

iv) Non-linear betatron transfer
The chromaticity and tune dependence on amplitude may be defined as input.

v) Non-linear synchrotron motion
Here an idealised RF station is assumed.

vi) Modulation effects
All known modulation effects are included, i.e. dispersion in the IPs, dispersion at the RF stations, longitudinal modulation of the interaction point, energy losses due to beam-beam deflection

vii) Lattice errors
The following types of error are included; phase advance between the IPs, spurious dispersions at the IPs, spurious beam separations and spurious variations of the beta functions at the IPs.

Not included:

i) Longitudinal and transverse wakefields
These were not included in the results published so far. However a modified version (as yet untested) exists which includes these effects. The longitudinal wakefield is particularly important as it causes more non-linearity in the synchrotron motion and can therefore drive modulation effects.

ii) Coherent beam-beam effects
Due to the numerology of the original code, coherent effects would only be properly simulated with one bunch per beam. The new version has the proper bunch numerology for observing coherent effects.

iii) β variation along the bunch collision length.
This effect was not included as it was considered unimportant for LEP where β^*/σ_s is around 6. Inclusion of this effect would require using the full three-dimensional potential equation which would significantly increase the required computer time.

(b) LEP II

Included:

i) Truly strong-strong

ii) Four-dimensional phase space
The longitudinal motion is neglected.

iii) Quantum excitation and damping

iv) Coherent beam-beam effects
The code was specifically written to study these effects.

Not included:

i) Non-linear betatron transfer

ii) Synchrotron motion
- and hence all modulation effects.

iii) Lattice errors

iv) β variation along the collision length

(c) PETRA

Included:

i) Six-di

ii) Quantu

iii) Approxi
These
synchro
interac

iv) Lattice
This wa
lattice

Not included

i) Strong-
All the
plot pe
the st
the bea

ii) Non-lin

iii) Non-lin

iv) Coheren

v) β varia

(d) PEGR

Included:

i) Approxi
Here th
verse d

ii) Six-dim

(c) PETRA

Included:

i) Six-dimensional phase space

ii) Quantum excitation and damping

iii) Approximated modulation effects
These effects are approximated due to the linearization of the synchrotron motion. The included effects are dispersion at the interaction points and longitudinal modulation of the IP.

iv) Lattice errors
This was the first published code which showed the importance of lattice errors.

Not included:

i) Strong-strong
All the results published in this work with the exception of one plot pertain to the weak-strong case. For the exceptional plot the strong-strong situation was approximated by renormalising the beam-beam kick once per transverse damping time.

ii) Non-linear betatron transfer

iii) Non-linear synchrotron motion

iv) Coherent beam-beam effects

v) β variation along the collision length

(d) CESR

Included:

i) Approximated strong-strong
Here the beam-beam kick is renormalised three times per transverse damping time.

ii) Six-dimensional phase space

iii) Quantum excitation and damping

iv) Some modulation effects
i.e. only dispersion at the IP is included.

Not included:

i) Non-linear betatron transfer

ii) Non-linear synchrotron motion

iii) Coherent beam-beam effects

iv β variation along the collision length

APPENDIX 4

TUNE MODULATION BETWEEN BEAM-BEAM INTERACTIONS

A given particle of one beam 'collides' with the centre of the counter-rotating beam $2k_b$ times per revolution. The actual position of this collision depends on the longitudinal position of the particle within the bunch relative to the synchronous particle (s), i.e. the actual position of collision ($\Delta\ell$), measured with respect to the nominal interaction point (where the centres of both beams collide)

$$\Delta\ell = -\frac{s}{2} \quad . \tag{A4.1}$$

The betatron phase difference between the synchronous particle and a particle $\Delta\ell$ from the IP is

$$\Delta\mu = \int_0^{\Delta\ell} \frac{ds}{\beta(s)}$$

and since

$$\beta(s) = \beta^* \left(1 + \frac{s^2}{\beta_*^2}\right)$$

$$\tan \Delta\mu = \frac{\Delta\ell}{\beta^*} = -\frac{s}{2\beta^*} \quad . \tag{A4.2}$$

The particle is longitudinally modulated at the synchrotron frequency, i.e. for small amplitude oscillations inside the RF bucket

$$s = \hat{s} \sin \omega_s t \quad . \tag{A4.3}$$

For $\Delta\ell \ll \beta$, (A4.2) and (A4.3) give

$$\Delta Q = \frac{\Delta\mu}{2\pi} \simeq -\frac{\hat{s} \sin\omega_s t}{4\pi\beta^*} \tag{A4.4}$$

and the change of ΔQ between collisions is

$$\Delta Q_{LM} = \frac{d\,\Delta Q}{dt} \frac{t_{rev}}{2k_b} = -\frac{Q_s\, \hat{s} \cos\omega_s t}{4\beta^* k_b} \quad . \tag{A4.5}$$

Equations (A4.4) and (A4.5) show that the maximum tune shift and change of tune shift between collisions for a particle with a (typical) longitudinal amplitude of σ_s are both proportional to

$$\frac{\sigma_s}{\beta^*} .$$

From (A4.5) the peak change of ΔQ per turn is

$$\Delta\hat{Q}/\text{turn} = -\frac{Q_s\hat{s}}{2\beta^*} \qquad \text{(A4.6)}$$

and since

$$Q_s\hat{s} = \frac{R}{\gamma_t^2}\left(\frac{\hat{\Delta E}}{E}\right)$$

$$\Delta Q/\text{turn} = -\frac{R}{2\gamma_t^2\beta^*}\left(\frac{\hat{\Delta E}}{E}\right) . \qquad \text{(A4.7)}$$

Consequently this effect gives an equivalent chromaticity of

$$Q'_{equiv} = -\frac{R}{2\gamma_t^2\beta^*} \qquad \text{(A4.8)}$$

which for LEP parameters (and $\beta^* = \sigma_s = 1.6$ cm) gives

$$Q'_{equiv} \simeq -50 .$$

1. M. Bassetti, P (Geneva, 7-11 J
2. F. Amman and D tors, Brookhav
3. J.T. Seeman, SL
4. R.H. Helm et a
5. A. Hofmann, J (1981), p. 239
6. M. Sands, SLAC-
7. D. Brandt and
8. T. Weiland, IE
9. A. Hofmann and Accelerators (
10. S. Kheifets, P
11. M. Bassetti an
12. A. Piwinski, P Geneva (7-11 J
see also
D. Degèle, R.
A. Piwinski, D
A. Piwinski, D
A. Piwinski, D
13. S. Peggs and Accelerators,
14. S. Myers, Nucl
see also
S. Myers, LEP
S. Myers, LEP
S. Myers, LEP
S. Myers, IEEE
15. E. Keil, Nuclea
16. M.H.R. Donald June 1979.
17. S. Myers, LEP
18. S. Myers, IEEE
19. A. Hutton, PEP-
20. J.M. Paterson,

REFERENCES

1. M. Bassetti, Proc. 11th Internat. Conf. on High Energy Accelerators (Geneva, 7-11 July 1980), Birkhäuser p. 650.

2. F. Amman and D. Ritson, 1961 Internat. Conf. on High Energy Accelerators, Brookhaven, p. 471, 1961.

3. J.T. Seeman, SLAC-PUB-3182, July 1983.

4. R.H. Helm et al., IEEE Trans. Nucl. Sci. NS-20, (1973), p. 900.

5. A. Hofmann, J. Jowett and S. Myers, IEEE Trans. Nucl. Sci. NS-28, (1981), p. 2392.

6. M. Sands, SLAC-121, Nov. 1970.

7. D. Brandt and B. Zotter, CERN LEP-TH/84-2, 1984.

8. T. Weiland, IEEE Trans. Nucl. Sci. NS-30, (Aug. 1983), pp. 2489-2491.

9. A. Hofmann and S. Myers, Proc. 11th Internat. Conf. on High Energy Accelerators (Geneva, 7-11 July 1980), pp. 610-614.

10. S. Kheifets, PETRA Note 119 (1.10.1976).

11. M. Bassetti and G. Erskine, CERN ISR-TH/80-06 (March 1980).

12. A. Piwinski, Proc. 11th Internat. Conf. on High Energy Accelerators, Geneva (7-11 July 1980) (Birkhäuser, 1980), p.751.
see also
D. Degèle, R. Kose, A. Piwinski, M. Placidi, DESY M-81/03, Mar. 1981.
A. Piwinski, DESY 80/131, Dec. 1980.
A. Piwinski, DESY M-81/31, Nov. 1981.
A. Piwinski, DESY 83-028, April 1983.

13. S. Peggs and R. Talman, Proc. 11th Internat. Conf. on High Energy Accelerators, Geneva (7-11 July 1980) (Birkhäuser, 1980), p. 754.

14. S. Myers, Nuclear Instr. and Methods 211, 1983 (pp. 263-282).
see also
S. Myers, LEP Note 188, October 1979.
S. Myers, LEP Note 310, June 1981.
S. Myers, LEP Note 400, August 1982.
S. Myers, IEEE Trans. Nucl. Sci. NS-28, June 1981 (pp. 2503-2505).

15. E. Keil, Nuclear Instr. and Methods 188, 1981 (pp. 9-14).

16. M.H.R. Donald and J.M. Paterson, IEEE Trans. Nucl. Sci., NS-26, June 1979.

17. S. Myers, LEP Notes 334, 344, November 1981.

18. S. Myers, IEEE Trans. Nucl. Sci., NS-30, August 1983 (pp. 2466-2468).

19. A. Hutton, PEP-Note-375, September 1982.

20. J.M. Paterson, private communication, July 1984.